A machine learning approach to tungsten prospectivity modelling using knowledge-driven feature extraction and model confidence

Christopher M. Yeomans[a,b,*], Robin K. Shail[a], Stephen Grebby[c], Vesa Nykänen[d], Maarit Middleton[d] and Paul A.J. Lusty[b]

[a]Camborne School of Mines, College of Engineering, Mathematics and Physical Sciences, University of Exeter, Penryn Campus, Penryn, Cornwall, TR10 9FE, UK

[b]British Geological Survey, Environmental Science Centre, Keyworth, Nottinghamshire, NG12 5GG, UK

[c]University of Nottingham, Nottingham Geospatial Institute, Innovation Park, Nottingham, NG7 2TU, UK

[d]Geological Survey of Finland, P.O. Box 77, FI-96101, Rovaniemi, Finland

Keywords

Machine learning; Mineral prospectivity modelling; Mineral exploration; Random Forest™; Tungsten; SW England

Abstract

Novel mineral prospectivity modelling presented here applies knowledge-driven feature extraction to a data-driven machine learning approach for tungsten mineralisation. The method emphasises the importance of appropriate model evaluation and develops a new Confidence Metric to generate spatially refined and robust exploration targets. The data-driven Random Forest™ algorithm is employed to model tungsten mineralisation in SW England using a range of geological, geochemical and geophysical evidence layers which include a depth to granite evidence layer. Two models are presented, one using standardised input variables and a second that implements fuzzy set theory as part of an augmented feature extraction step. The use of fuzzy data transformations mean feature extraction can incorporate some user-knowledge about the mineralisation into the model. The commonly subjective approach is guided using the Receiver Operating Characteristics (ROC) curve tool where transformed data are compared to known training samples. The modelling is conducted using 34 known true positive samples with 10 random sets of randomly generated true negative samples to test the random effect on the model. The two models have similar accuracy but show different spatial distributions when identifying highly prospective targets. Areal analysis shows that the fuzzy-transformed model is a better discriminator and highlights three areas of high prospectivity that are not previously known. The Confidence Metric, derived from model variance, is employed to further evaluate the models. The new metric is useful for refining exploration targets and highlighting the most robust areas for follow-up investigation. The fuzzy-transformed model is shown to contain larger areas of high model confidence compared to the model using standardised variables. Finally, legacy mining data, from drilling reports and old mine descriptions, is used to further validate the fuzzy-

transformed model and gauge the depth of potential deposits. Descriptions of mineralisation corroborate that the targets generated in these models could be undercover at depths of less than 300 m. In summary, the modelling workflow presented herein provides a novel integration of knowledge-driven feature extraction with data-driven machine learning modelling, while the newly derived Confidence Metric generates reliable mineral exploration targets.

---

1. Introduction

The use of Machine Learning Algorithms (MLAs) for mineral prospectivity modelling has been driven by the increasing size of individual datasets and the range of data types available for mineral exploration. MLAs are computationally efficient and can deal with large, high-dimensional input datasets, non-Gaussian distributions, and generate robust exploration targets from few training samples (Emmanuel John M. Carranza and Laborte, 2015a, 2015b; Rodriguez-Galiano et al., 2015). The approach requires some *a priori* data to train the model indicating it is a data-driven method. However, the number of training samples can be <20 which is a significant improvement compared to other data-driven methods such as Weights-of-Evidence (Emmanuel John M. Carranza and Laborte, 2015b). MLAs are now commonplace in mineral prospectivity modelling. The Random Forest, Support Vector Machine and Artificial Neural Network algorithms are regularly implemented and it is the Random Forest MLA that is proving most effective in comparison studies (Rodriguez-Galiano et al., 2015; Sun et al., 2019).

Prospectivity modelling is often conducted at a large-scale, encompassing national or regional areas to determine new exploration targets. Studies have become increasingly effective due to investment in the acquisition of high-resolution airborne geophysical, satellite and geochemical datasets over large areas (Bahiru and Woldai, 2016; Kreuzer et al., 2010). Furthermore, the commitment from state geological surveys to undertake airborne geophysical surveys and geochemical baseline studies for both mineral exploration and environmental purposes has led to high-quality datasets often being freely available.

Classical prospectivity modelling has been dominated by the Weights-of-Evidence and Fuzzy Logic methods. Whilst MLAs may be a more effective data-driven method, the Fuzzy Logic technique is knowledge-based and founded on fuzzy set theory. The approach allows user-knowledge to be incorporated into the model through various data transformations chosen by the user (An et al., 1991; Bonham-Carter, 1994; Zadeh, 1965). The advantage of this is the ability to weight different data and to introduce some dependencies between variables that may be inferred by the user but not captured in the data. Until recently, this technique has been considered highly subjective but work by Nykänen et al. (2015, 2017) provides a means of guiding the data processing. By using fuzzy transformations as part of the feature extraction step in MLA modelling, some user-knowledge can be introduced to potentially improve a data-driven analysis.

MLAs also offer key post-hoc metrics to evaluate the model beyond the standard accuracy metrics. These include model variance and information entropy, which have been investigated, respectively, by Cracknell and Reading (2013) and Kuhn et al. (2018). Cracknell

and Reading (2013) demonstrated the value of assessing model variance for a multi-class problem when mapping lithology to highlight fault zones, whereas Kuhn et al. (2018) used information entropy to guide field sampling campaigns to assist with geological mapping. These metrics are useful for highlighting potentially erroneous aspects of a model, which cannot be found when evaluating a model through a single accuracy metric, but have not been implemented within a mineral prospectivity modelling framework.

Herein, we demonstrate the use of fuzzy set theory for feature extraction, as well as post-hoc metrics, for tungsten mineralisation in SW England using a Random Forest MLA. We explore how incorporating knowledge-driven principles as part of feature extraction within a data-driven modelling workflow can improve the final results and compare this to a model using standardised (zero mean and equal variance) input variables. Furthermore, the models are spatially evaluated using model variance and a newly derived Confidence Metric which are applied to generate robust targets for mineral exploration with a refined area. Finally, legacy mining data are used to further validate new targets and give a depth estimate to mineralisation.

1.1. Prospectivity modelling and machine learning

MLAs are versatile tools for mineral prospectivity modelling but can be misused if the data preparation and model evaluation are inappropriate. Therefore, data preparation, also known as feature extraction, as well as methods of evaluating models through accuracy statistics and other metrics, are briefly considered below.

1.1.1. Feature extraction

The advent of high-resolution datasets of various types has meant that mineral prospectivity models often include high numbers of input variables which increase the dimensionality. Minimising the number of variables means redundant data can be reduced to avoid skewing the results, therefore improving classification accuracy and reducing computation times (Witten et al., 2017). The other reason for selecting a minimum number of variables is to mitigate the “curse-of-dimensionality”, also known as the “Hughes effect” (Hughes, 1968) whereby the number of training samples required to capture data variance increases disproportionately with the number of variables. This is an important consideration when only a small number of training samples are available. Feature extraction and careful data processing is of paramount importance to minimise both data redundancy and the number of input variables.

The process of manipulating variables to enhance desirable characteristics is known as feature extraction. Commonly, the aim is to highlight a particular range in the original data, through simple statistics or combining with other variables (e.g. multiplication or ratios), to amplify interactions between different variables (Henery, 1994a, 1994b). Some of these options may also have the benefit of mitigating noise and removing correlated data (Hastie et al., 2009). Another option is to highlight particular features using data transformations or image enhancements. There are a broad range of transformations which can be tailored to the task and, when used appropriately with an appropriate MLA, a high degree of accuracy can be achieved (Sukumar et al., 2014).

In mineral prospectivity modelling, it is common for initial data preparation to include computing the distance from particular features as an example of feature extraction (e.g. proximity-to structures). Many prospectivity models attempt to use factor analysis, principal component analysis or the singularity method to process data, which are other forms of feature extraction (Abedi et al., 2013; C. Wang et al., 2017; J. Wang et al., 2017; Wang et al., 2018; Zhao et al., 2015). The transformation and weighting of data is also part of the feature extraction process, of which fuzzy membership and fuzzy operators in a Fuzzy Logic approach are an example of feature extraction by transforming the data and weighting desirable features within the study area.

1.1.2. Model evaluation

The output for mineral prospectivity modelling using MLAs is often a binary classification but it is the class probabilities, the likelihood that a pixel is classified correctly, that are of value when considering prospectivity (Harris et al., 2015). It is good practice to evaluate the accuracy of the prospectivity models, most commonly through the Receiver Operating Characteristics (ROC) curve tool (Agterberg and Bonham-Carter, 2005; Fawcett, 2006; Nykänen, 2008; Robinson and Larkins, 2007) which uses *True Positives* (TP), *True Negatives* (TN), *False Positives* (FP) and *False Negatives* (FN) to determine a range of metrics including *Sensitivity* (Equation 1) and *Specificity* (Equation 2). The ROC curve tool plots *Sensitivity* against *1 - Specificity* and this can be used to calculate the Area-Under-Curve (AUC).

$$Sensitivity = \frac{TP}{TP+FN} \quad (1)$$

$$Specificity = \frac{TN}{TN+FP} \quad (2)$$

MLAs also have further evaluation metrics which are often overlooked, such as the calculation of model variance from class probabilities that can be subsequently presented spatially as a map (Cracknell and Reading, 2013; Kohavi and Wolpert, 1996). Model variance was implemented as part of lithological mapping by Cracknell and Reading (2013) in the Broken Hill area of New South Wales, Australia where higher variance was an indicator for the presence of fault zones and was termed “the upside of uncertainty”. A further derivative of model variance is information entropy used by Kuhn et al. (2018) for similar purposes and shown to be useful in geological mapping campaigns to target areas for follow-up work that may be poorly understood.

There have been limited attempts to apply these tools to mineral prospectivity modelling. There is often a predilection for distilling a model to a single accuracy metric, however, this is not ideal especially with spatial data where some aspects of the model may be well-constrained and other components highly suspect. Model variance can spatially highlight where the model is failing and provide useful information to the user that can feedback to initial feature extraction. By incorporating the spatial distribution of model variance into the evaluation process, the user can enhance the analysis and mitigate the potential limitations of a single accuracy metric.

1.2. Geological framework

SW England hosts a world-class tin-tungsten province and provides an excellent case study site for prospectivity modelling due to the recent acquisition of high-resolution airborne

geophysical and geochemical datasets (Beamish et al., 2014; British Geological Survey, 2016). The regional geology (Figure 1) is dominated by low-grade regionally metamorphosed Devonian-Carboniferous successions that were deformed during the Variscan Orogeny; these were subseqently intruded by the Early Permian Cornubian Batholith (Leveridge and Hartley, 2006; Scrivener, 2006; Shail and Leveridge, 2009; Simons et al., 2016). The batholith is closely associated with a tin-tungsten orefield that has also been exploited for copper, zinc, lead, silver, antimony, arsenic, uranium and a number of other subordinate metals (Jackson et al., 1989). Tungsten mineralisation is governed by Variscan and post-Variscan regional tectonic and structural development and the coeval magmatic and magmatic-hydrothermal evolution of the batholith; these are briefly discussed below.

1.2.1. Regional tectonics and structural geology

The regional structural geological evolution records two episodes of deformation (D1 and D2) relating to Variscan convergence and collision (e.g. Sanderson and Dearman, 1973; Alexander and Shail, 1996; Rattey and Sanderson, 1984). These were associated with the development of NNW-directed thrust faults and NNW-SSE transfer faults within Devonian and Carboniferous successions (Coward and Smallwood, 1984; Dearman, 1970, 1963; Shail and Alexander, 1997).

NNW-SSE post-convergence extension (D3) commenced in the latest Carboniferous and brought about reactivation of Variscan thrust faults and the generation of new higher angle extensional faults through much of the Early Permian (Figure 2; Shail and Wilkinson, 1994; Alexander and Shail, 1996, 1995). Subsequent and successive minor ENE-WSW (D4) and NNW-SSE (D5) Permian intraplate shortening events are recognised (Hobson and Sanderson, 1983; Rattey and Sanderson, 1984; Shail and Alexander, 1997). The D3-D5 events spanned batholith construction and mineralisation and their brittle expression, as faults and tensile fractures, were essential for the migration of magmatic-hydrothermal fluids and the development of lodes and sheeted veins (Shail and Alexander, 1997; Shail and Wilkinson, 1994). Tungsten deposits form in cuspate bodies of granite and only extend a short distance into the country rock (Ball et al., 1998; Hosking and Trounson, 1959; Jackson et al., 1989). These deposits are commonly proximal to NW-SE major faults (e.g. Hemerdon, Redmoor, Cligga Head) which may control mineralisation either directly or through subordinate structures.

1.2.2. Permian granite batholith

Five different granite types have been identified across the region: G1, two-mica granite; G2, muscovite granite; G3, biotite granite; G4, tourmaline granite; G5, topaz granite (Simons et al., 2016). The association between granite type and mineral prospectivity is not well-constrained; granite types close to surface are commonly older than, and unrelated to, the lode mineralisation they host. Nevertheless, tourmaline granites (G4) are common in areas of significant tin mineralisation and have been interpreted as the precursor differentiated magmas that released Sn-bearing magmatic-hydrothermal fluids (e.g. Müller et al., 2006). Topaz granites (G5) host very low-grade disseminated Sn-W-Tb-Nb mineralisation but have been inferred to be the source of substantial tourmalinisation haloes and associated Sn-W mineralisation (Manning and Hill, 1990). There is an association between muscovite granites

(G2), typically present as small stocks and interpreted as a differentiation product of G1 granites, and W mineralisation (Simons et al., 2017, 2016).

1.2.3. Tungsten mineralisation and exploration

SW England has a number of tungsten deposits which have been described in detail, such as the Cligga Head (Hall, 1971; Moore and Jackson, 1977) and St Michael's Mount (Dominy et al., 1995) sheeted vein systems and the Hemerdon stockwork (Cameron, 1951; Dines, 1956; Shail et al., 2017); the latter recently operated by Wolf Minerals Ltd (2015-2018). It is important to note that almost all tungsten is hosted in wolframite with only trace amounts of scheelite. Figure 3 shows all known tungsten occurrences that are reported in the BGS GeoIndex (2018) (https://www.bgs.ac.uk/mineralsuk/data/mineocc.html). Additional tungsten occurrences are known and described in Dines (1956) but are not readily available in digital form and are instead used for qualitative evaluation.

Exploration has been selective and focused around known tungsten deposits. Andrews et al. (1987) conducted soil geochemical studies around the Hemerdon deposit which involved three transects and identified geochemical anomalies although no follow up trenching is known. Geochemical exploration at Redmoor, which made use of an extensive diamond and percussive drilling campaign as well as samples of float (rock fragments in soil), attempted to define an alteration halo (Newall, 1994; Newall and Newall, 1989). The work used factor analysis to identify a "mineralisation factor" for the elements As, Cu, W , Sn, Na* and Zr (where * indicates a negative correlation). Beer et al. (1986) identify clear geochemical anomalies for tungsten, based on percussive drilling along traverses, nearby to the Castle-an-Dinas tungsten lode. The Mulberry and Wheal Prosper area was investigated by Bennett et al. (1981) who found both tungsten and tin anomalies in proximity to calc-silicate units in the Meadfoot Group in soil geochemistry. Regional investigations were undertaken by Moore and Camm (1982) and James and Moore (1985) using space-borne Landsat MSS and Seasat data to map regional structures associated with tungsten mineralisation.

2. Data and Methods

The workflow illustrated in Figure 4 shows the steps required to incorporate knowledge-based feature extraction into a data-driven modelling workflow and generate spatially refined robust targets for mineral exploration. These include defining the conceptual deposit model, initial data preparation, feature extraction using fuzzy transformations and machine learning modelling. Models generated through the Random Forest MLA are evaluated through model variance and a Confidence Metric to highlight spatially refined and robust mineral exploration targets.

2.1. Conceptual tungsten deposit model

The conceptual deposit model for the target mineral deposit enables the user to identify key exploration criteria. These are represented by evidence layers, generated from available datasets. Regional geological, geochemical and geophysical datasets have been incorporated in this work to identify tungsten mineralisation in SW England. The contribution of these evidence layers to the conceptual deposit model is described below.

Prior mineral exploration and geological investigations provide a substantial body of research on which to build a regional conceptual deposit model for tungsten mineralisation in SW England (Andrews et al., 1987; Ball et al., 2002, 1998; Hall, 1971; Hosking and Trounson, 1959; Jackson et al., 1989; Moore and Camm, 1982; Moore and Jackson, 1977; Newall, 1994; Newall and Newall, 1989; Shail et al., 2017). Based on these observations, a conceptual deposit model has been developed to capture the common characteristics of known tungsten deposits (Figure 5). The model is based on a range of available geological, geochemical and geophysical datasets. Geological data comprises the mapped extent of granite plutons based on British Geological Survey 1:50 000 data and a depth to granite layer determined from the LiDAR Digital Terrain Model (DTM) and the granite surface model, based on regional gravity data, created by Willis-Richards and Jackson (1989). Geochemical datasets include soil and stream-sediment data from the G-BASE survey (British Geological Survey, 2016), Tellus South West airborne geophysical surveys (Beamish et al., 2014; Ferraccioli et al., 2014) and lineament data derived by Yeomans et al. (2019).

The evidence layers generated from these datasets have been prepared within the ESRI ArcGIS Desktop software package. These data were resampled to a common extent and resolution based on the airborne geophysical data (40 m pixels) and standardised to zero mean and equal variance; as is usual in many machine learning approaches (Camps-Valls et al., 2007; Cracknell and Reading, 2015, 2014; Hastie et al., 2009). The data preparation steps for each layer are presented in the Supplementary Information (S1).

2.1.1. Geological evidence layers

The geological exploration criteria defined here are based on the observation that tungsten mineralisation generally occurs, in granites or their host rocks, close to the margins of "cuspate" granite bodies or cupolas, at the roof of the batholith (Ball et al., 1998; Beer et al., 1975; Dominy et al., 1995; Hosking and Trounson, 1959). An evidence layer for proximity-to granite was prepared using the British Geological Survey 1:50 000 shapefile data to capture the XY locations of granite contacts. A proximity-to granite layer was also prepared to capture the depth to the granite contact in areas that may have blind mineralisation. The granite surface from the 3D model created by Willis-Richards and Jackson (1989) is subtracted from the LiDAR DTM and included as a proximity-to layer that captures the distance to granite in Z (depth) to identify shallow granite bodies. Due to some areas of the model protruding above surface, the evidence layer was classified into seven groups to allow down-weighting of the protruding areas.

Structural information was also included based on observations by Shail et al. (2017) using regional lineament data derived from the airborne geophysics by Yeomans et al. (2019). A proximity-to structures layer using a Euclidean distance algorithm was prepared based on NW-SE lineaments with lengths > 1200 m. Furthermore, a density map of all NW-SE structures was created to capture areas of high fracturing that may be favourable for mineralisation.

2.1.2. Geochemical evidence layers

Regional soil and stream-sediment geochemical data from the G-BASE survey (British Geological Survey, 2016) were used to derive geochemical evidence layers. The soil data were collected from between 0 and 0.2 m depth and sieved at 2 mm. Stream-sediment data

were analysed using X-ray Fluorescence Spectroscopy with no digestive reagent. Strict Quality Assessment and Quality Control was conducted by the British Geological Survey prior to release through the G-BASE survey; detailed by Wragg et al. (2018).

Geochemical evidence layers have been created through an Inverse-Distance Weighting (IDW) algorithm based on preparation steps by Carranza (2010) and are summarised in Table 1. The geochemical data includes both soil and stream-sediment datasets for all evidence layers discussed below excluding the K/(Zr/Eu). This ratio is exclusive to the stream-sediment data due the lack of analysis for rare earth elements during analysis of the soil data. These data are considered in three groups representing mineralisation, aureole and granite geochemistry.

For mineralisation geochemistry, information on the target metal, W, is included as well as Sn due to this common association (Cameron, 1951; Dines, 1956; Hall, 1971; Jackson et al., 1989; Moore and Jackson, 1977). The inclusion of As, Bi, Sb, Na*, Rb and Cs (where * indicates a negative correlation) is based on the previous exploration campaigns.

As, Bi and Sb are used as indicators for mineralisation where tungsten and tin may not be prevalent. They occur at distance from the deposit (Andrews et al., 1987), therefore, these elements may be a vector element in soil geochemistry for mineralisation at depth (or laterally) where the main tungsten mineralisation is undercover and assuming there has been minimal soil transport. It is worth noting that Sb is considered to not a reliable indicator element by Ball et al. (2002) but is included to determine its importance in this particular study.

The inclusion of Na*, Rb and Cs and ratios such as K/Rb* and K/Cs* is based on aureole geochemistry and alteration in mineralised country rocks surrounding granite cupolas (Ball et al., 1998; Newall and Newall, 1989). Other elements that are enriched include Li and F (Andrews et al., 1987; Ball et al., 1998; Newall, 1994; Newall and Newall, 1989), but there are insufficient analyses for these elements across the region and they have therefore not been included.

Lithogeochemical evidence layers are focused on granite types and these are defined using two ratios. Ti/Sn* is useful for determining a general granite signature (Ball et al., 1984, 1998) but fails to separate specific granite types. By interrogating geochemical data from Simons et al. (2016), an indicator ratio has been found, K/(Zr/Eu), to separate the G2 granite from other granite types (Figure 6); albeit with some close associations with the G1a type. Other useful ratios have been identified such Zr/Fe_2O_3, Nb/Zr and Ba/Rb but are largely indistinct for separating G2 granites (Simons et al., 2016). Potential indicator elements for G2 granite types include Be and Li (Simons et al., 2017); however, these are not included in the available soil and stream-sediment geochemical datasets for the region.

2.1.3. Geophysical evidence layers

The geophysical evidence layers defined in the conceptual deposit model incorporate airborne radiometric data from the Tellus South West project. The magmatic-hydrothermal aureole around granite plutons in SW England is highlighted by the ratio of tan^{-1}(K/eU*). It is therefore included to capture hydrothermal alteration where elevated uranium concentrations indicate that mineralising fluids may have circulated; as with geochemical ratios the evidence layer is an inverse relationship. The inverse tangent function is applied

to the ratio and results in a non-linear normalisation with the data scaled from -1.57 to +1.57 which limits the affects of outliers and potentially infinite values (IAEA, 2003; Schetselaar, 2002).

2.2. Fuzzy feature extraction

The data processing discussed in this section concerns the gridded raster data used for the input variables of the modelling. The data processing was conducted in ArcSDM 5, maintained by the Geological Survey of Finland (GTK, 2019), which compiles various tools for mineral prospectivity modelling. It includes the ROC curve tool that is used for data assessment and validation. The first machine learning prospectivity model uses the initial standardised variables. The second model uses fuzzy-transformed variables that required further processing, using guided fuzzy set theory. The aim of this is to assess whether combining user-knowledge through fuzzy membership and fuzzy operator transformation enhances model performance.

2.2.1. Fuzzy membership transformation

The subjective nature of fuzzy set theory and the Fuzzy Logic method can be circumvented by refining input variables using the ROC curve tool developed by Nykänen et al. (2015, 2017). The approach provides a quantitative metric for assessing subjective aspects of the Fuzzy Logic technique, namely the application of the fuzzy membership function and fuzzy operators such as *FuzzyOR* (An et al., 1991; Bonham-Carter, 1994). The tool optimises the output of these functions and operators and at the same time provides information on the spatial correlation of input variables with known deposits. In turn, the correlation of an input layer can be used to indicate whether it is correctly included as part of the conceptual deposit model. Further, by repeating the ROC curve analysis 10 times, Nykänen et al. (2017) demonstrate that a more robust metric is obtained that highlights the variability in the AUC statistic when using randomly generated non-deposit samples.

The method applied here used an iterative approach to assess the fuzzy membership function using the ROC curve tool and refine each input variable. The fuzzy membership function transforms initial evidence layers by determining a *spread* and *midpoint*. Once a variable was determined to be ascending or descending; e.g. the target values are small or large, respectively, the *spread* and *midpoint* was optimised to create a layer with the best AUC value. Note that the Proximity-to Granite in Z was generated using the Table of Contents (TOC) function from the ArcSDM 5 package. A list of the final input variables and the optimised parameters used for the fuzzy membership functions is given in Table 2. A complete table of all the iterations generated is presented in the Supplementary Information (S1).

The averaged results of 10 different ROC curve analyses provides a robust metric for determining the validity of the applied fuzzy membership function. It is clear that some input variables have a much higher AUC than others. Nykänen et al. (2017) suggest there is value in the inclusion of a variable even where AUC values are close to 0.5 (random correlation) because it may provide mutually beneficial information to a subsequent combination of variables later in the analysis, e.g. through fuzzy operators.

2.2.2. Fuzzy operator combinations

Following fuzzy membership transformation, some input variables were combined into single layers to not only enhance the variable but to also assist with dimensionality reduction in the model. Elements with geochemical analyses in the form of both soil and stream-sediment data were integrated into single variables to represent the overall anomalies for that element (Figure 7). The same approach was also applied to geochemical ratios, with the exception of K/(Zr/Eu) as this was only created from stream-sediment geochemistry due to the omission of REE analysis for the soil data. A visual inspection of the data was conducted prior to integration to ensure that values in each variable were comparable.

The *fuzzyOR* operator is considered to be the best tool to combine two elements or ratios into a single input variable to maximise potential anomalies (Bonham-Carter, 1994) and reduce dimensionality in the model and it is used here to maximise indications of geochemical anomalies from both datasets. These were subsequently reassessed using the ROC curve tool and new AUC values were calculated (Table 3). For W, Sn, As and Na, this results in a synergistic effect where the AUC is greater than both AUC values for the individual datasets. For Bi, Sb, Rb, Cs, K/Cs, K/Rb and Ti/Sn, the AUC values fall between the lower and upper values derived for the original datasets.

2.3. Machine learning methods

Various MLAs are available for prospectivity modelling, however, it is the Random Forest algorithm that has consistently proven to be highly effective in comparison to Support Vector Machines and Artificial Neural Networks (Carranza and Laborte, 2016; Emmanuel John M. Carranza and Laborte, 2015a, 2015b; Rodriguez-Galiano et al., 2015; Sun et al., 2019). For this reason, two Random Forest models are presented for prospectivity modelling, one using standardised variables with no transformation and the other using variables transformed using the guided fuzzy set theory approach of Nykänen et al. (2015, 2017). An advantage of the machine learning approach to mineral prospectivity modelling is the evaluation metrics available for each algorithm. Many classification methods allow the probability of a pixel being correctly classified (the class probabilities) to be interrogated. For mineral prospectivity modelling, class probabilities are often presented as the final result but these can be further manipulated through model variance (Cracknell and Reading, 2013; Kohavi and Wolpert, 1996) to evaluate the model using a newly derived Confidence Metric.

2.3.1. Training and validation data

A set of known tungsten occurrences was compiled from the Mineral Occurrence Database maintained by the BGS GeoIndex (2018). A total of 34 known tungsten occurrences are recorded in the region and were used as true positive samples. These true positive samples were randomly subset 70:30 into 23 training and 11 validation data.

True negative samples are also necessary to accurately model and validate unfavourable areas. An equal number of true negative samples were generated to ensure balanced training classes and minimise error rates (Mellor et al., 2015). These samples were created through random sampling of the study area as outlined by Nykänen et al. (2015). A

minimum buffer of 400 m was applied to minimise spatial correlation with either true positive samples, or other true negative samples. Furthermore, 10 different sets of random samples were generated to assess the effect of randomisation on the validation results as suggested by Nykänen et al. (2017). Therefore, the procedure of validation is to combine the true positive samples with a different set of true negative samples 10 times and subsequently calculate the mean, median and standard deviation of the AUC results. This approach provides information on the variability caused by random points and of sensitivity whilst minimising the chance of a biased true negative sample set affecting model validation. The 10 sets of 34 true negative samples were merged and subset 70:30 into 23 training and 11 validation data per set. Training data from the first random set were included in the modelling.

2.3.2. Prospectivity modelling

Prospectivity modelling was performed using a combination of GIS, the ArcSDM package and the *R* statistical computing language (R Core Team, 2019). A binary MLA classification model was created where two classes were used (unfavourable and favourable) to determine a simple class probability model. MLA models were implemented using the *caret* (Kuhn et al., 2019), *raster* (Hijmans, 2019) and *rgdal* (Bivand et al., 2019) packages. A full description of the *R* workflow is presented in the Supplementary Information (S2).

The Random Forest method is an ensemble decision tree machine learning algorithm (Breiman, 2001). The approach combines multiple binary-split trees which limits overfitting that can occur through multi-split trees (Hastie et al., 2009). The Random Forest algorithm utilises multiple randomised decision trees (the forest) where the random effect is controlled by the user-defined *mtry* value; a means of subsetting the input variables used to initiate the trees (Breiman, 2001). The *mtry* value can be defined using a random or grid search to find the best value, or by calculating the square root of the number of input variables (Belgiu and Drăguţ, 2016; Breiman, 2001; Gislason et al., 2006). A further parameter must be set, *ntree*, which dictates the number of binary trees in the forest and controls the reproducibility of the results. Based on a review by Belgiu and Drăguţ (2016), *ntree* is commonly set to 500 for most classification problems using remote sensing data. Emmanuel John M. Carranza and Laborte (2015b) increased *ntree* to 20 000 in order to achieve stable predictions and lower the prediction error for a training set of 12 samples. Given the comparably small training sample size in this study (23 training samples and 11 validation samples), the *ntree* value of 20 000 was adopted for this study.

A total of 28 variables are included in the standardised model (see Table 2) and 17 included in the fuzzy-transformed model whereby all duplicate geochemical elements have been combined using the *fuzzyOR* operator (see Table 3). All fuzzy-transformed and combined data were included in the modelling process despite the potentially low relevance of Sb. The inclusion of Sb is due to its minor positive correlation with known deposits that may still contribute some relevant information.

2.3.3. The Confidence Metric

Spatial evaluation of the model can be undertaken by calculating the model variance (Equation 3) of the class probabilities to derive an uncertainty value (Kohavi and Wolpert, 1996). The technique was implemented by Cracknell and Reading (2013) to show areas

where the classification is less reliable. In this study, model variance is exploited to determine whether favourable targets are truly robust in the mineral prospectivity model. By combining model variance and the class probabilities into the new Confidence Metric using Equation 4, exploration targets can be refined to highlight the areas of highest confidence in the model.

$$model\ variance\ (v) = \frac{1-\sum p_c^2}{1-\sum\left(\frac{1}{c}\right)} \quad (3)$$

Where p_c is the class probability for each class per pixel and c is the total number of classes.

$$confidence\ (p_{conf}) = \frac{(p_c - v)_i - min(p_c - v)}{max(p_c - v) - min(p_c - v)} \quad (4)$$

Where i indicates a per pixel subtraction.

By subtracting the model variance, the values of pixels with high uncertainty are reduced accordingly, leaving only the most reliable areas with high class probabilities. In some cases, this can reduce the value to less than zero and, for the purposes of comparison, Equation 4 normalises the output to a range of 0 to 1.

2.3.4. Areal evaluation

The spatial distribution of the prospectivity is quantitatively evaluated using areal analysis. Total areal extents are calculated for each level of prospectivity (unfavourable through to highly favourable) as a sum of the area for each level and as a percentage of total area of the model. The analysis provides a quantitative assessment of the spatial distribution of the class probabilities for each model and the associated confidence. The proportion of pixels at each prospectivity level are compared to determine which model is better at discriminating prospective areas.

2.3.5. Depth evaluation

The rich mining history of SW England means that there is an extensive repository of data but the quality of digital records is highly variable. Legacy mining data is available through the British Geological Survey from the Mineral Exploration & Investigation Grants Act (MEIGA) records and published works such as Dines (1956). These resources are used to further evaluate the depth at which deposits may occur.

3. Results and Discussion

The results of the MLA modelling using both feature extraction methods are presented below. These are assessed based on the AUC values from ROC curve analysis and further evaluated using the Confidence Metric, areal analysis and legacy mining data. These evaluation techniques, respectively, aim to generate robust targets, compare the spatial attributes of the model and to give an indication of whether targets are likely to reside at surface or at depth.

3.1. Tungsten prospectivity modelling results

The results of the modelling using standard and fuzzy input variables are presented in Figure 8 and Figure 9. Each figure comprises the binary classification of all prospective areas, the class probability for a cell being classified as prospective and the confidence map derived using the Equation 4.

The class map for the prospectivity model shows broad areas of prospective areas for tungsten mineralisation due to the binary classification. The Random Forest class probability map is therefore more useful as it demonstrates the likelihood that a location is prospective. For Figure 8 and Figure 9, the data have been categorised to show only values greater than 0.5 in colour, this is to indicate that anything below this value would have been classified as unfavourable in the binary classification.

The class probability map for the standardised variables (Figure 8) shows a good correlation with known tungsten occurrences. Areas of high favourability are constrained to areas of known deposits marked as W-Y in Figure 8b, which include the Camborne-Redruth district, the St Austell district and the east Bodmin-Kit Hill area, respectively. However, no highly favourable areas are identified that were not previously known and only limited areas have been identified as favourable.

Figure 9 shows the class probability map for the fuzzy-transformed variables that identifies highly favourable areas over known tungsten occurrences similar to those in Figure 9b including the Cligga Head (Z) and the margin of the north Bodmin Granite (E). Additional areas include the Breage district (A), the southern margin of the Bodmin Granite (B) and some discrete targets along the eastern margin of the Dartmoor Granite (C) which are new prospects. The map also shows broader areas of favourable prospectivity away from main targets which are of interest.

The ROC curve tool was used to validate these models and generate a quantitative measure of accuracy for the binary classification. A summary of the validation results from the ROC curve analysis is included in Table 4. The average AUC values for both class probability models are very high and not significantly different. It is unsurprising that both models have such similar AUC values due to sharing the same initial evidence layers and the invariance of the Random Forest algorithm to changes in scale imparted by the fuzzy membership transformation. Furthermore, the similarity in AUC values underlines that the use of training samples with the ROC curve tool during feature extraction has not overly biased the model. However, the reduction in dimensionality from 28 to 17 input variables in the fuzzy-transformed model appears to have provided no significant improvements to the modelling.

Despite the minimal difference in AUC values, the lack of new highly prospective targets in the standardised variable model is disappointing. Nevertheless, the greater number of new targets in the fuzzy-transformed model indicates that the incorporation of user-knowledge through fuzzy-transformed variables during feature extraction has refined target identification within a data-driven Random Forest modelling approach.

3.2. Target confidence

The use of model variance (Equation 3) has been demonstrated by Cracknell and Reading (2013) where areas of high variance were spatially correlated with fault zones between classified lithologies. Here, the uncertainty associated with model variance is manipulated using Equation 4 and transformed into a measure of confidence for potentially prospective areas.

The confidence maps for each model shown in Figure 8c and Figure 9c reveal highly favourable and favourable areas that are not only significantly refined in area, but define more reliable targets. Any area shown to be >0.5 in terms of confidence should be compared to the class probability map to determine its favourability and those areas with high class probabilities and high confidence are likely to be robust. Therefore, the confidence map helps to elucidate highly favourable and favourable areas and interpret reliable exploration targets.

3.3. Model comparison from areal evaluation

The two Random Forest models presented here can also be assessed to determine the prospectivity by area. Models for class probability and confidence have been assessed in terms of area in Table 5. These show the total area and normalised area for each class shown in Figure 8 and Figure 9.

The total areas are similar for each model and small discrepancies are due to rounding errors. The class probability model for standardised variables shows a greater proportion of the study area having some degree of prospectivity (>0.5). In contrast, the class probability model for the fuzzy-transformed variables shows a smaller proportion of the study area to be prospective (>0.5) but the areas that are identified have a greater degree of prospectivity; the most prospective areas (>0.8) accounts for 3.7% of the total area compared to 2% when using standardised variables. Similarly, the confidence model for both methods has been assessed. If a value of >0.5 is taken as a reasonable confidence level, 3.2% and 5.2% of the models for standard variables and fuzzy-transformed variables, respectively, can be considered to be robust.

The results from this analysis would infer that the fuzzy-transformed variables give an overall greater confidence when generating exploration targets compared to the standardised variables. By revisiting Table 3, it can be seen that the combination of W, Sn, As and Na has a mutually beneficial effect on the AUC values compared to the prior values for the individual soil and stream-sediment geochemical layers. These mutually beneficial combinations are likely to improve the MLA model and enhance target delineation.

Evaluation using legacy mining data

New targets were identified from the Random Forest model using fuzzy-transformed variables. These include the Breage district, the southern margin of the Bodmin Granite and some discrete targets along the eastern margin of the Dartmoor Granite labelled A, B and C, respectively (Figure 9b). These are further highlighted in Figure 10 alongside additional legacy data to further assess the fuzzy-transformed variable model.

In the Breage district (Figure 10a), historic mining records indicate tungsten mineralisation was intersected at depth at Prospidnick on the SW margin of the Carnmenellis Granite and at Great Wheal Fortune on the eastern margin of the Tregonning-Godolphin Granite (Dines, 1956). Furthermore, a borehole was drilled in the area that intersected tungsten and tin mineralisation (Ball et al., 1984); this is also missing from BGS GeoIndex (2018).

Studies conducted under MEIGA are not recorded in the BGS GeoIndex (2018). The mineralisation along the southern margin of the Bodmin Granite (Figure 10b) was investigated by Consolidated Gold Fields Ltd as part of regional tungsten exploration study funded by MEIGA in 1972. Tungsten and tin anomalies were identified in streams and follow-up soil sampling was also conducted. A drilling campaign along the southern margin of the granite was conducted which intersected tungsten mineralisation but grades and tonnages were deemed uneconomic at the time.

Targets identified in Figure 10c along the eastern margin of the Dartmoor Granite require further follow-up work. No records of tungsten have been found, however, four mines are inferred by Dines (1956) to become uneconomic with depth with respect to tin and it was suggested that other “uneconomic” metals may exist but are not described further. One of these mines exists outside of the surface crop of the granite and intersects the granite margin at approximately 90 m below surface.

The use of these additional resources helps validate the mineral prospectivity model. The reference to tungsten mineralisation found in old mines and former drilling projects suggests that some of these targets may be within a few hundred metres of surface. This further supports the model for identifying blind deposits and the inclusion of the proximity-to granite in Z evidence layer is likely to be important and high resolution gravity measurements may improve the analysis significantly.

Conclusions

Mineral prospectivity modelling has been conducted using a data-driven Random Forest MLA approach for tungsten in SW England. A particular focus has been put on feature extraction and the use of initial variables that were standardised to zero mean and equal variance compared to those that were further processed using knowledge-driven fuzzy membershipa and fuzzy overlay functions.

The two models presented here have similar accuracies based on ROC curve analysis but show different spatial distributions of prospectivity in the region. The model that uses standardised variables only identifies areas of high prospectivity (>0.9) proximal to the training data. The second model, using fuzzy-transformed input variables, identifies three new highly prospective targets that were previously unidentified in the training data. The improvement in target generation is directly attributable to the use of knowledge-driven feature extraction techniques within a data-driven MLA framework.

These models are enhanced using model variance to derive a new Confidence Metric. The Confidence Metric is a simple calculation to infer where class probabilities are most robust. These are presented as a map that can be combined with the initial class probabilities to

determine the most reliable targets. The approach results in spatially refined and robust mineral exploration targets that can allow for a more focus follow-up field campaign.

The models have been further evaluated by an areal analysis showing that the fuzzy-transformed model is a better discriminator for prospective areas compared to the standardised variable model due to the mutually beneficial effect of combining geochemical layers such as W, Sn, As and Na during feature extraction. Also, the fuzzy-transformed model has greater confidence and generates greater proportion of robust targets by area based on the Confidence Metric. By conducting model evaluation in this way, two models with the same statistical accuracy but different spatial distributions can be better understood. This study underlines how single accuracy metrics can be fallible when applied to spatial datasets.

Finally, the use of legacy mining data further reinforces the strength of the model where all three new target areas have potential economic mineralisation either through direct sampling or inferred from mine descriptions. Further, the legacy mining data suggests that the targets generated may be within 300 m of surface. This would indicate the "Proximity-to granite in Z" evidence layer derived from regional gravity data is valuable and that new discoveries of tungsten mineralisation in SW England may be enhanced by a new high resolution gravity survey.

Acknowledgements

CMY would like to thank Dr Charles Moon for his constructive comments on an early draft. The work was completed as part of doctoral research by CMY funded by the British Geological Survey (S267) and the Natural Environment Research Council (NERC) GW4+ Doctoral Training Partnership (NE/L002434/1) in collaboration with the Geological Survey of Finland (GTK). Data used in this study are available from the Tellus South West project website (www.tellusgb.ac.uk). PL publishes with the permission of the Executive Director, British Geological Survey (UKRI).

References

Abedi, M., Norouzi, G.H., Torabi, S.A., 2013. Clustering of mineral prospectivity area as an unsupervised classification approach to explore copper deposit. Arabian Journal of Geosciences 6, 3601–3613. https://doi.org/10.1007/s12517-012-0615-5

Agterberg, F.P., Bonham-Carter, G.F., 2005. Measuring the performance of mineral-potential maps. Natural Resources Research 14, 1–17. https://doi.org/10.1007/s11053-005-4674-0

Alexander, A.C., Shail, R.K., 1996. Late- to post-Variscan structures on the coast between Penzance and Pentewan, South Cornwall. Proceedings of the Ussher Society 9, 72–78.

Alexander, A.C., Shail, R.K., 1995. Late Variscan structures on the coast between Perranporth and St. Ives, Cornwall. Proceedings of the Ussher Society 8, 398–404.

An, P., Moon, W.M., Rencz, A., 1991. Application of fuzzy set theory to integrated mineral exploration. Canadian Jounral of Exploration 27, 1–11. https://doi.org/10.3997/2214-4609.201410970

Andrews, M.J., Ball, T.K., Fuge, R., Nicholson, R.A., Peachey, D., 1987. Trace elements in soils around the Hemerdon tungsten deposit, Devon; implications for exploration. Proceedings of the Ussher Society 6, 536–541.

Bahiru, E.A., Woldai, T., 2016. Integrated geological mapping approach and gold mineralization in Buhweju area, Uganda. Ore Geology Reviews 72, 777–793. https://doi.org/10.1016/j.oregeorev.2015.09.010

Ball, T.K., Basham, I.R., Charoy, B., 1984. Petrogenesis of the Bosworgey granitic cusp in the SW England tin province and its implications for ore mineral genesis. Mineralium Deposita 19, 70–77. https://doi.org/10.1007/BF00206599

Ball, T.K., Fortey, N.J., Beer, K.E., 2002. Aspects of the lithogeochemistry of arsenic, antimony and bismuth in South West England. Geoscience in South-West England 10, 352–357.

Ball, T.K., Fortey, N.J., Beer, K.E., 1998. Alkali metasomatism from Cornubian granite cupolas. Geoscience in South-West England 9, 171–177.

Beamish, D., Howard, A., Ward, E.K., White, J., Young, M.E., 2014. Tellus South West airborne geophysical data.

Beer, K.E., Ball, T.K., Bennett, M.J., 1986. Mineral investigations near Bodmin, Cornwall. Part 5 - The Castle-an-Dinas wolfram lode. Mineral Reconnaissance Programme Report, British Geological Survey. No.82; Mineral Reconnaissance Programme Report, British Geological Survey. No.82.

Beer, K.E., Burley, A.J., Tombs, J.M., 1975. The concealed granite roof in south-west Cornwall. Mineral Reconnaissance Programme Report, Institute of Geological Sciences, No.1 [Unpublished]; Mineral Reconnaissance Programme Report, Institute of Geological Sciences, No.1 [Unpublished].

Belgiu, M., Drăguţ, L., 2016. Random forest in remote sensing: A review of applications and future directions. ISPRS Journal of Photogrammetry and Remote Sensing 114, 24–31. https://doi.org/10.1016/j.isprsjprs.2016.01.011

Bennett, M.J., Beer, K.E., Jones, R.C., Turton, K., Rollin, K.E., Tombs, J.M.C., Patrick, D.J., 1981. Mineral investigations near Bodmin, Cornwall. Part 3 - The Mulberry and Wheal Prosper area. Mineral Reconnaissance Programme Report. Institute of Geological Sciences, No. 48; Mineral Reconnaissance Programme Report. Institute of Geological Sciences, No. 48.

BGS GeoIndex, 2018. Mineral Occurrence Database.

Bivand, R., Keitt, T., Rowlingson, B., 2019. rgdal: Bindings for the 'Geospatial' Data Abstraction Library.

Bonham-Carter, G.F., 1994. Geographic information systems for geoscientists: modelling with GIS, First. ed. Elsevier Science Ltd, Kidlington, UK.

Breiman, L., 2001. Random forests. Machine Learning 45, 5–32. https://doi.org/10.1023/A:1010933404324

British Geological Survey, 2016. G-BASE for Southwest England.

Cameron, J., 1951. The Geology of the Hemerdon wolfram mine, Devon. Transactions of the Institution of Mining and Metallurgy 6L, 1–14.

Camps-Valls, G., Bandos Marsheva, T.V., Zhou, D., 2007. Semi-supervised graph-based hyperspectral image classification. IEEE Transactions on Geoscience and Remote Sensing 45, 3044–3054. https://doi.org/10.1109/TGRS.2007.895416

Carranza, E.J.M., 2010. Mapping of anomalies in continuous and discrete fields of stream sediment geochemical landscapes. Geochemistry: Exploration, Environment, Analysis 10, 171–187. https://doi.org/10.1144/1467-7873/09-223

Carranza, E.J.M., Laborte, A.G., 2016. Data-Driven Predictive Modeling of Mineral Prospectivity Using Random Forests: A Case Study in Catanduanes Island (Philippines). Natural Resources Research 25, 35–50. https://doi.org/10.1007/s11053-015-9268-x

Carranza, E.J.M., Laborte, A.G., 2015a. Data-driven predictive mapping of gold prospectivity, Baguio district, Philippines: Application of Random Forests algorithm. Ore Geology Reviews 71, 777–787. https://doi.org/10.1016/j.oregeorev.2014.08.010

Carranza, E.J.M., Laborte, A.G., 2015b. Random forest predictive modeling of mineral prospectivity with small number of prospects and data with missing values in Abra (Philippines). Computers and Geosciences 74, 60–70. https://doi.org/10.1016/j.cageo.2014.10.004

Coward, M.P., Smallwood, S., 1984. An interpretation of the Variscan tectonics of SW Britain. Geological Society, London, Special Publications 14, 89–102. https://doi.org/10.1144/GSL.SP.1984.014.01.08

Cracknell, M.J., Reading, A.M., 2015. Spatial-Contextual Supervised Classifiers Explored: A Challenging Example of Lithostratigraphy Classification. IEEE Journal of Selected Topics in Applied Earth Observations and Remote Sensing 8, 1371–1384. https://doi.org/10.1109/JSTARS.2014.2382760

Cracknell, M.J., Reading, A.M., 2014. Geological mapping using remote sensing data: A comparison of five machine learning algorithms, their response to variations in the spatial distribution of training data and the use of explicit spatial information. Computers and Geosciences 63, 22–33. https://doi.org/10.1016/j.cageo.2013.10.008

Cracknell, M.J., Reading, A.M., 2013. The upside of uncertainty: Identification of lithology contact zones from airborne geophysics and satellite data using random forests and support vector machines. Geophysics 78, 113—–126. https://doi.org/10.1190/GEO2012-0411.1

Dearman, W.R., 1970. Some aspects of the tectonic evolution of South-West England. Proceedings of the Geologists' Association 81, 483–491. https://doi.org/10.1016/S0016-7878(70)80009-8

Dearman, W.R., 1963. Wrench-faulting in Cornwall and south Devon. Proceedings of the Geologists' Association 74, 265–287. https://doi.org/10.1016/S0016-7878(63)80023-1

Dines, H.G., 1956. The Metalliferous mining region of south-west England. Economic Memoirs of the Geological Survey of Great Britain.

Dominy, S.C., Camm, G.S., Bussell, M.A., Scrivener, R.C., Halls, C., 1995. A review of tin stockwork mineralization in the south-west England orefield. Proceedings of the Ussher Society 8, 368–373.

Fawcett, T., 2006. An introduction to ROC analysis. Pattern Recognition Letters 27, 861–874. https://doi.org/10.1016/j.patrec.2005.10.010

Ferraccioli, F., Gerard, F., Robinson, C., Jordan, T., Biszczuk, M., Ireland, L., Beasley, M., Vidamour, A., Barker, A., Arnold, R., Dinn, M., Fox, A., Howard, A., 2014. LiDAR based Digital Terrain Model (DTM) data for South West England. https://doi.org/10.5285/e2a742df-3772-481a-97d6-0de5133f4812

Gislason, P.O., Benediktsson, J.A., Sveinsson, J.R., 2006. Random forests for land cover classification. Pattern Recognition Letters 27, 294–300. https://doi.org/10.1016/j.patrec.2005.08.011

GTK, 2019. ArcSDM.

Hall, A., 1971. Greisenisation in the granite of Cligga Head, Cornwall. Proceedings of the Geologists' Association 82, 209–230.

Harris, J.R., Grunsky, E., Behnia, P., Corrigan, D., 2015. Data- and knowledge-driven mineral prospectivity maps for Canada's North. Ore Geology Reviews 71, 788–803.

Hastie, T., Tibshirani, R., Friedman, J., 2009. The Elements of Statistical Learning, Springer series in statistics. Springer New York, New York, NY. https://doi.org/10.1007/978-0-387-84858-7

Henery, R.J., 1994a. Classification, in: Michie, D., Spiegelhalter, D.J., Taylor, C.C. (Eds.), Machine Learning, Neural and Statistical Classification. Ellis Horwood, New York, pp. 6–16.

Henery, R.J., 1994b. Methods for Comparison, in: Michie, D., Spiegelhalter, D.J., Taylor, C.C. (Eds.), Machine Learning, Neural and Statistical Classification. Ellis Horwood, New York, pp. 107–124.

Hijmans, R.J., 2019. raster: Geographic Data Analysis and Modeling.

Hobson, D.M., Sanderson, D.J., 1983. Variscan Deformation in Southwest England, in: Hancock, P.L. (Ed.), The Variscan Fold Belt in the British Isles. Adam Hilger Ltd, Bristol, pp. 108–129.

Hosking, K.F.G., Trounson, J.H., 1959. The mineral potential of Cornwall, in: Non-Ferrous Mining in Great Britain and Ireland. Institution of Mining; Metallurgy Symposium, London, pp. 335–369.

Hughes, G.F., 1968. On the Mean Accuracy of Statistical Pattern Recognizers. IEEE Transactions on Information Theory 14, 55–63. https://doi.org/10.1109/TIT.1968.1054102

760 IAEA, 2003. Guidelines for radioelement mapping using gamma ray spectrometry data,
761 IAEA-TECDOC-1363. International Atomic Energy Agency, Vienna, Austria.

762 Jackson, N.J., Willis-Richards, J., Manning, D.A.C., Sams, M.S., 1989. Evolution of the
763 Cornubian ore field, Southwest England; Part II, Mineral deposits and ore-forming
764 processes. Economic Geology 84, 1101–1133.

765 James, J.M., Moore, J.M., 1985. Multi-seasonal imagery studies for geological mapping and
766 prospecting in cultivated terrain of S.W. England, in: Fourth Thematic Conference: "Remote
767 Sensing for Exploration Geology", San Francisco, California, April 1-4, 1985. San Francisco,
768 California, pp. 475–484.

769 Kohavi, R., Wolpert, D.H., 1996. Bias plus variance decomposition for zero-one loss
770 functions, in: Proceedings of the 13th International Conference on Machine Learning
771 (Icml96), Bari, Italy. pp. 275–283.

772 Kreuzer, O.P., Markwitz, V., Porwal, A.K., McCuaig, T.C., 2010. A continent-wide study of
773 Australia's uranium potential. Part I: GIS-assisted manual prospectivity analysis. Ore Geology
774 Reviews 38, 334–366. https://doi.org/10.1016/j.oregeorev.2010.08.003

775 Kuhn, M., Wing, J., Weston, S., Williams, A., Keefer, C., Engelhardt, A., Cooper, T., Mayer, Z.,
776 Kenkel, B., the R Core Team, Benesty, M., Lescarbeau, R., Ziem, A., Scrucca, L., Tang, Y.,
777 Candan, C., Hunt., T., 2019. caret: Classification and Regression Training.

778 Kuhn, S., Cracknell, M.J., Reading, A.M., 2018. Lithologic mapping using Random Forests
779 applied to geophysical and remote-sensing data: A demonstration study from the Eastern
780 Goldfields of Australia. Geophysics 83, B183–B193. https://doi.org/10.1190/geo2017-0590.1

781 Leveridge, B.E., Hartley, A.J., 2006. The Varisan Orogeny: the development and deformation
782 of Devonian/Carboniferous basins in SW England and South Wales, in: Brenchley, P.J.,
783 Rawson, P.F. (Eds.), The Geology of England and Wales. The Geological Society, London, pp.
784 225–256.

785 Manning, D.A.C., Hill, P.I., 1990. The petrogenetic and metallogenetic significance of topaz
786 granite from the southwest England orefield. Geological Society of America Special Paper
787 246, 51–69.

788 Mellor, A., Boukir, S., Haywood, A., & Jones, S. (2015). Exploring issues of training data
789 imbalance and mislabelling on random forest performance for large area land cover
790 classification using the ensemble margin. ISPRS Journal of Photogrammetry and Remote
791 Sensing, 105, 155–168. https://doi.org/10.1016/j.isprsjprs.2015.03.014

792 Moore, J.M., Camm, S., 1982. Interactive enhancement of Landsat Imagery for structural
793 mapping in tin-tungsten prospecting: a case history of the S.W. England Orefield (U.K.), in:
794 International Symposium on Remote Sensing of Environment, Second Thematic Conference,
795 Remote Sensing for Exploration Geology. Fort Worth, Texas, December 6 - 10, 1982, pp.
796 727–740.

797 Moore, J.M., Jackson, N., 1977. Structure and mineralization in the Cligga granite stock,
798 Cornwall. Journal of the Geological Society, London 133, 467–480.
799 https://doi.org/10.1144/gsjgs.133.5.0467

Müller, A., Seltmann, R., Halls, C., Siebel, W., Dulski, P., Jeffries, T., Spratt, J., Kronz, A., 2006. The magmatic evolution of the Land's End pluton, Cornwall, and associated pre-enrichment of metals. Ore Geology Reviews 28, 329–367. https://doi.org/10.1016/j.oregeorev.2005.05.002

Newall, P.S., 1994. An integrated geochemical approach to investigate the concealed mineralization at the Redmoor Sn/W sheeted vein deposit, east Cornwall, England. Journal of Southeast Asian Earth Sciences 10, 109–130. https://doi.org/10.1016/0743-9547(94)90013-2

Newall, P.S., Newall, G.C., 1989. Use of lithogeochemistry as an exploration tool at Redmoor sheeted-vein complex, east Cornwall, southwest England. Transactions of the Institution of Mining and Metallurgy 98, B162–B174.

Nykänen, V., 2008. Radial Basis Functional Link Nets Used as a Prospectivity Mapping Tool for Orogenic Gold Deposits Within the Central Lapland Greenstone Belt, Northern Fennoscandian Shield. Natural Resources Research 17, 29–48. https://doi.org/10.1007/s11053-008-9062-0

Nykänen, V., Lahti, I., Niiranen, T., Korhonen, K., 2015. Receiver operating characteristics (ROC) as validation tool for prospectivity models - A magmatic Ni-Cu case study from the Central Lapland Greenstone Belt, Northern Finland. Ore Geology Reviews 71, 853–860. https://doi.org/10.1016/j.oregeorev.2014.09.007

Nykänen, V., Niiranen, T., Molnhár, F., Lahti, I., Korhonen, K., Cook, N., Skyttä, P., 2017. Optimizing a Knowledge-driven Prospectivity Model for Gold Deposits Within Peräpohja Belt, Northern Finland. Natural Resources Research 26, 571–584. https://doi.org/10.1007/s11053-016-9321-4

Rattey, P.R., Sanderson, D.J., 1984. The structure of SW Cornwall and its bearing on the emplacement of the Lizard Complex. Journal of the Geological Society, London 141, 87–95.

R Core Team, 2019. R: A Language and Environment for Statistical Computing.

Robinson, G.R., Larkins, P.M., 2007. Probabilistic prediction models for aggregate quarry siting. Natural Resources Research 16, 135–146. https://doi.org/10.1007/s11053-007-9039-4

Rodriguez-Galiano, V., Sanchez-Castillo, M., Chica-Olmo, M., Chica-Rivas, M., 2015. Machine learning predictive models for mineral prospectivity: An evaluation of neural networks, random forest, regression trees and support vector machines. Ore Geology Reviews 71, 804–818. https://doi.org/10.1016/j.oregeorev.2015.01.001

Sanderson, D.J., Dearman, W.R., 1973. Structural zones of the Variscan fold belt in SW England, their location and development. Journal of the Geological Society, London 129, 527–536. https://doi.org/10.1144/gsjgs.129.5.0527

Schetselaar, E., 2002. Petrogenetic interpretation from gamma-ray spectrometry and geological data: the Arch Lake zoned peraluminous granite intrusion, Western Canadian shield. Exploration Geophysics 33, 35–43. https://doi.org/10.1071/EG02035

Scrivener, R.C., 2006. Cornubian granites and mineralization of SW England, in: Brenchley, P.J., Rawson, P.F. (Eds.), The Geology of England and Wales. The Geological Society, London, pp. 257–268.

Shail, R.K., Alexander, A.C., 1997. Late Carboniferous to Triassic reactivation of Variscan basement in the western English Channel: evidence from onshore exposures in south Cornwall. Journal of the Geological Society, London 154, 163–168. https://doi.org/10.1144/gsjgs.154.1.0163

Shail, R.K., Leveridge, B.E., 2009. The Rhenohercynian passive margin of SW England: Development, inversion and extensional reactivation. Comptes Rendus Geoscience 341, 140–155.

Shail, R.K., Wilkinson, J.J., 1994. Late-to Post-Variscan extensional tectonics in south Cornwall. Proceedings of the Ussher Society 8, 262–270.

Shail, R., McFarlane, J., Hassall, L., Thiel, H., Stock, T., Smethurst, M., Tapster, S., Scrivener, R., Leveridge, B., Simons, B., 2017. The geological setting of the Hemerdon W–Sn deposit. Transactions of the Institutions of Mining and Metallurgy, Section B: Applied Earth Science 7453, 1. https://doi.org/10.1080/03717453.2017.1306292

Simons, B., Andersen, J.C., Shail, R.K., Jenner, F., 2017. Fractionation of Li, Be, Ga, Nb, Ta, In, Sn, Sb, W and Bi in the peraluminous Early Permian Variscan granites of the Cornubian Batholith: precursor processes to magmatic-hydrothermal mineralisation. Lithos 278-281, 491–512. https://doi.org/10.1016/j.lithos.2017.02.007

Simons, B., Shail, R.K., Andersen, J.C., 2016. The petrogenesis of the Early Permian Variscan granites of the Cornubian Batholith: Lower plate post-collisional peraluminous magmatism in the Rhenohercynian Zone of SW England. Lithos 260, 76–94. https://doi.org/10.1016/j.lithos.2016.05.010

Sukumar, M., Venkatesan, N., Babu, C.N.K., 2014. A review of various lineament detection techniques for high resolution satellite images. International Journal of Advanced Research in Computer Science and Software Engineering 4, 72–78.

Sun, T., Chen, F., Zhong, L., Liu, W., Wang, Y., 2019. GIS-based mineral prospectivity mapping using machine learning methods: a case study from Tongling ore district, eastern China. Ore Geology Reviews 109, 26–49. https://doi.org/10.1016/j.oregeorev.2019.04.003

Wang, C., Rao, J., Chen, J., Ouyang, Y., Qi, S., Li, Q., 2017. Prospectivity mapping for "Zhuxi-type" copper-tungsten polymetallic deposits in the Jingdezhen region of Jiangxi Province, South China. Ore Geology Reviews 89, 1–14. https://doi.org/10.1016/j.oregeorev.2017.05.022

Wang, J., Zuo, R., Caers, J., 2017. Discovering geochemical patterns by factor-based cluster analysis. Journal of Geochemical Exploration 181, 106–115. https://doi.org/10.1016/j.gexplo.2017.07.006

Wang, W., Cheng, Q., Zhang, S., Zhao, J., 2018. Anisotropic singularity: A novel way to characterize controlling effects of geological processes on mineralization. Journal of Geochemical Exploration 189, 32–41. https://doi.org/10.1016/j.gexplo.2017.07.019

Willis-Richards, J., Jackson, N.J., 1989. Evolution of the Cornubian Ore Field, Southwest England: Part I. Batholith Modeling and Ore Distribution. Economic Geology 84, 1078–1100.

Witten, I.H., Frank, E., Hall, M.A., Pal, C.J., 2017. Data Mining: Practical Machine Learning Tools and Techniques, Fourth. ed. Morgan Kaufmann (Elsevier).

Wragg, J., Cave, M., Hamilton, E., Lister, T., 2018. The Link between Soil Geochemistry in South-West England and Human Exposure to Soil Arsenic. Minerals 8, 570. https://doi.org/10.3390/min8120570

Yeomans, C.M., Middleton, M., Shail, R.K., Grebby, S., Lusty, P.A.J., 2019. Integrated Object-Based Image Analysis for semi-automated geological lineament detection in southwest England. Computers & Geosciences 123, 137–148 [Available Online November 2018]. https://doi.org/10.1016/j.cageo.2018.11.005

Zadeh, L.A., 1965. Fuzzy sets. Information and Control 8, 338–353. https://doi.org/10.1016/S0019-9958(65)90241-X

Zhao, J., Zuo, R., Chen, S., Kreuzer, O.P., 2015. Application of the tectono-geochemistry method to mineral prospectivity mapping: A case study of the Gaosong tin-polymetallic deposit, Gejiu district, SW China. Ore Geology Reviews 71, 719–734. https://doi.org/10.1016/j.oregeorev.2014.09.023

Figure Captions

Figure 1: Summary geology of SW England showing Devonian-Carboniferous sedimentary host rock in grey, granite outcrop in red and depth-to granite contours based on the granite surface model by Willis-Richards and Jackson (1989). Black lines represent regional lineaments derived by Yeomans et al. (2019) from Tellus South West airborne geophysical data.

Figure 2: Schematic illustrations of the kinematics and structures generated during Permian-Triassic extension (D3-D6). After Shail and Alexander (1997).

Figure 3: Schematic outline of extractive areas in SW England showing tin, copper and tungsten. Data from BGS GeoIndex (2018) are based on historic production values from known mines, deposit and prospect localities as well as reported mineral showings and panned concentrates. Important tungsten producers are labeled based on data from Dines (1956) and Jackson et al. (1989). Key mining areas are highlighted on the map: a = St Just, b = Camborne-Redruth, c = Breage, d = St Austell, e = Bodmin, f = Tamar Valley.

Figure 4: Mineral prospectivity modelling workflow for combining knowledge-based feature extraction into a data-driven machine learning approach to generate spatially refined and robust targets for mineral exploration.

Figure 5: Conceptual deposit model for tungsten mineralisation in SW England showing the main geological phenomena targeted by the prospectivity modelling.

Figure 6: Granite geochemistry showing the distribution of granite types based on the classification by Simons et al. (2016). The G2 granite is distinct having a low Zr/Eu ratio and high K, however, the G1a granite shows a similar signature.

Figure 7: (A) interpolated stream-sediment geochemical data for tungsten that have been transformed using the fuzzy membership function. (B) interpolated soil geochemical data for tungsten that have been transformed using the fuzzy membership function. (C) resulting tungsten geochemical data that have been combined using the fuzzyOR operator to emphasis key anomalies.

Figure 8: (A) Classification map (B) Class probability map and (C) confidence map for the standardised variables Random Forest prospectivity model. Classes show the two class scenario where 1 is unprospective and 2 is prospective. The class probability and confidence models are categorised to show 0.9 to 1 as highly favourable (red), 0.8 to 0.9 as favourable (amber), 0.65 to 0.8 as less favourable (turquoise), 0.5 to 0.65 as possibly favourable (blue) and <0.5 as unfavourable (grey).

Figure 9: (A) Classification map (B) Class probability map and (C) confidence map for the fuzzy-transformed variables Random Forest prospectivity model. Classes show the two class scenario where 1 is unprospective and 2 is prospective. The class probability and confidence models are categorised to show 0.9 to 1 as highly favourable (red), 0.8 to 0.9 as favourable (amber), 0.65 to 0.8 as less favourable (turquoise), 0.5 to 0.65 as possibly favourable (blue) and <0.5 as unfavourable (grey).

Figure 10: Key target locations based on the class probability map from the fuzzy-transformed variables model. The Breage district is shown in (A) where drilling projects and mining legacy data are shown to validate the targets. Targets around the Bodmin Granite are shown in (B) with new areas validated by a drilling report. The eastern margin of the Dartmoor Granite is shown in (C) where mining legacy data are proximal to favourable targets.

Table Captions

Table 1: Geochemical data included as evidence for tungsten mineralisation. The geochemistry are grouped into three phenomena describing the mineralisation, granite aureole and granite type.

Table 2: AUC values for evidence layers transformed using fuzzy membership functions. The AUC values are calculated from ten ROC curve analyses using randomly generated false occurrences.

Table 3: AUC values for combined geochemical elements and ratios, calculated from ten ROC curve analyses using randomly generated false occurrences. These are compared to the geochemical values for original datasets from soil and stream-sediment (SS) data. In some cases (W, Sn, As, Na) the combination is mutually beneficial.

Table 4: AUC values for each Random Forest™ prospectivity model. Calculated from ten ROC curve analyses using randomly generated false occurrences. The key parameters have been included for each model.

Table 5: Area assessment for both standardised and fuzzy-transformed models. The data have been calculated in a GIS to show the area accounted for by each class as a sum and a percentage for both the class probability (Prob) map and confidence (Conf) maps. Small discrepancies are attributed to rounding errors.

Figure 1

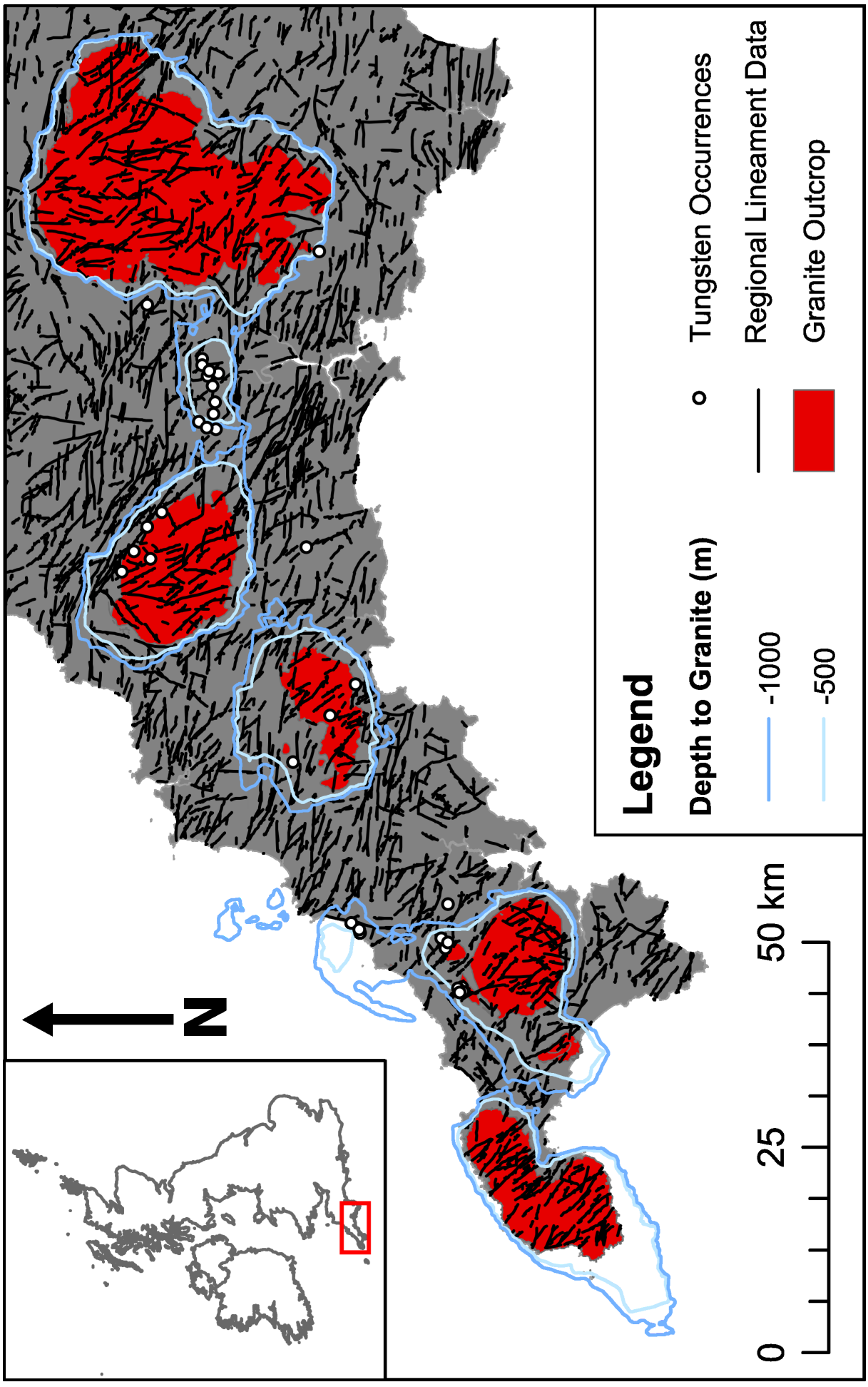
Legend
Depth to Granite (m)
-1000
-500
Tungsten Occurrences
Regional Lineament Data
Granite Outcrop
N
0
25
50 km

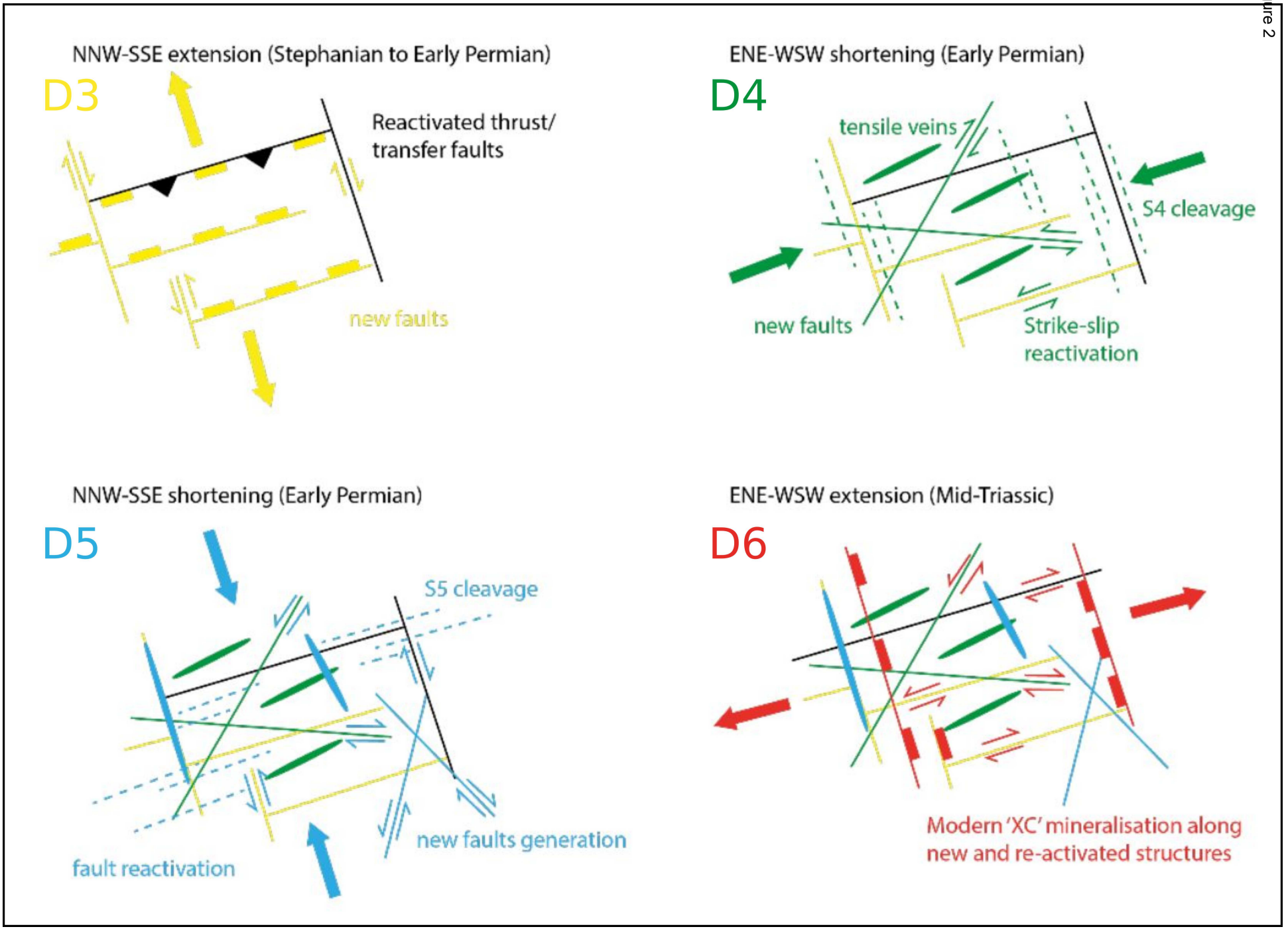
NNW-SSE extension (Stephanian to Early Permian)
D3
Reactivated thrust/
transfer faults
new faults
ENE-WSW shortening (Early Permian)
D4
tensile veins
S4 cleavage
new faults
Strike-slip
reactivation
NNW-SSE shortening (Early Permian)
D5
S5 cleavage
new faults generation
fault reactivation
ENE-WSW extension (Mid-Triassic)
D6
Modern 'XC' mineralisation along
new and re-activated structures

Figure 3

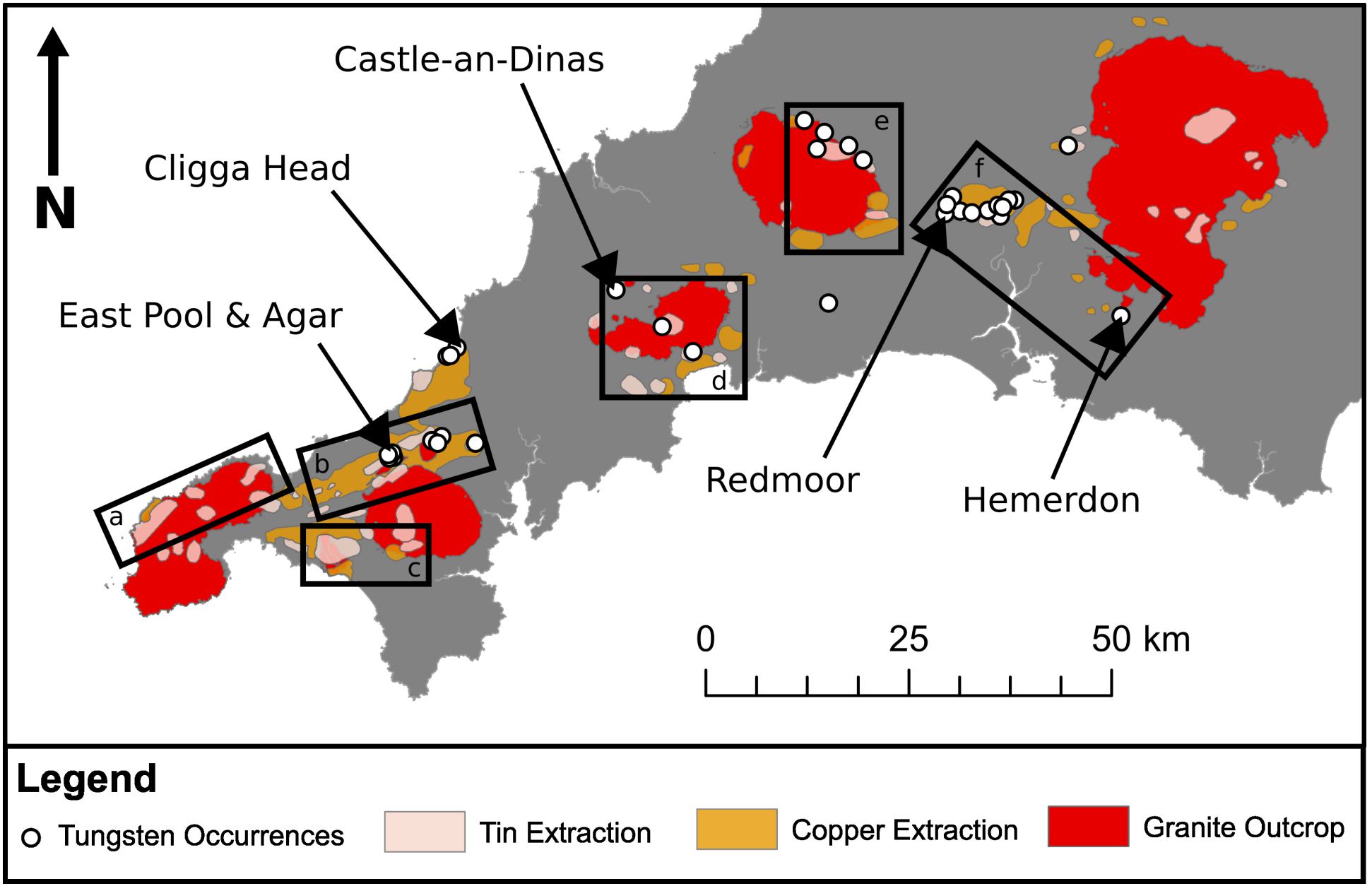
N
Castle-an-Dinas
Cligga Head
East Pool & Agar
Redmoor
Hemerdon
a
b
c
d
e
f
0
25
50 km
Legend
Tungsten Occurrences
Tin Extraction
Copper Extraction
Granite Outcrop

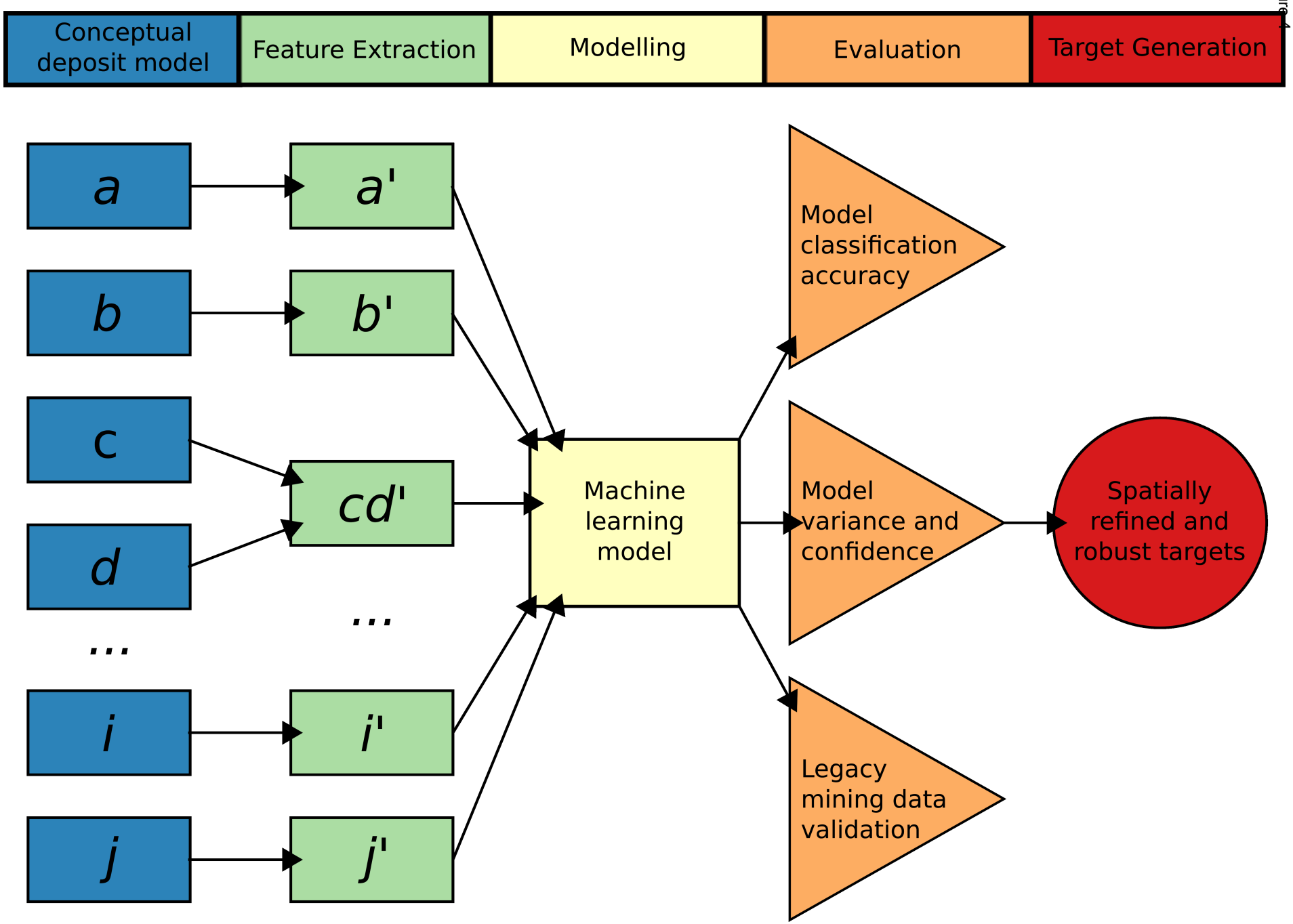
Conceptual deposit model
Feature Extraction
Modelling
Evaluation
Target Generation
a
b
c
d
...
i
j
a'
b'
cd'
...
i'
j'
Machine learning model
Model classification accuracy
Model variance and confidence
Legacy mining data validation
Spatially refined and robust targets

Figure 4

Figure 5

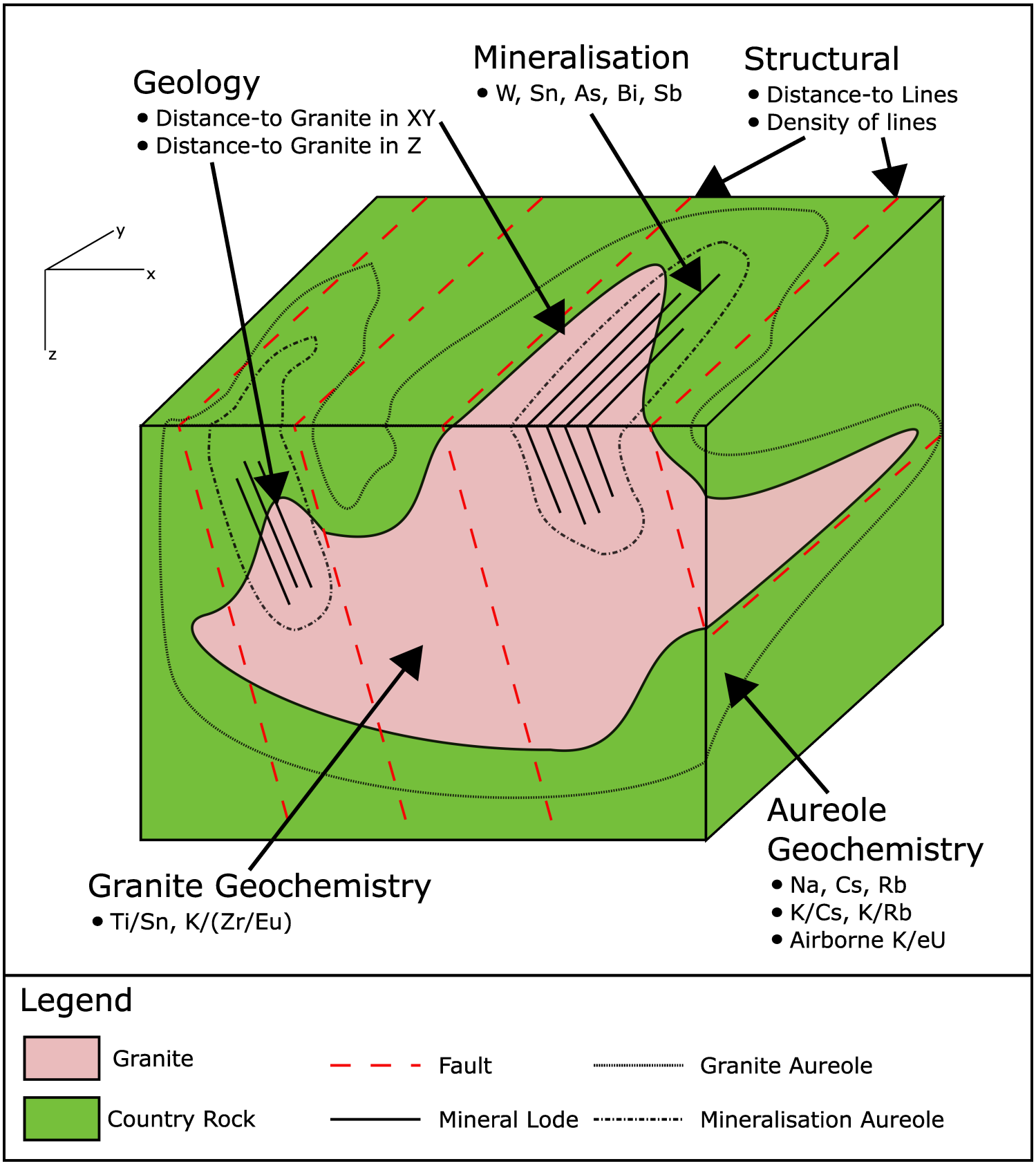
Geology
• Distance-to Granite in XY
• Distance-to Granite in Z
Mineralisation
• W, Sn, As, Bi, Sb
Structural
• Distance-to Lines
• Density of lines
y
x
z
Granite Geochemistry
• Ti/Sn, K/(Zr/Eu)
Aureole Geochemistry
• Na, Cs, Rb
• K/Cs, K/Rb
• Airborne K/eU
Legend
Granite
Country Rock
Fault
Mineral Lode
Granite Aureole
Mineralisation Aureole

Figure 6

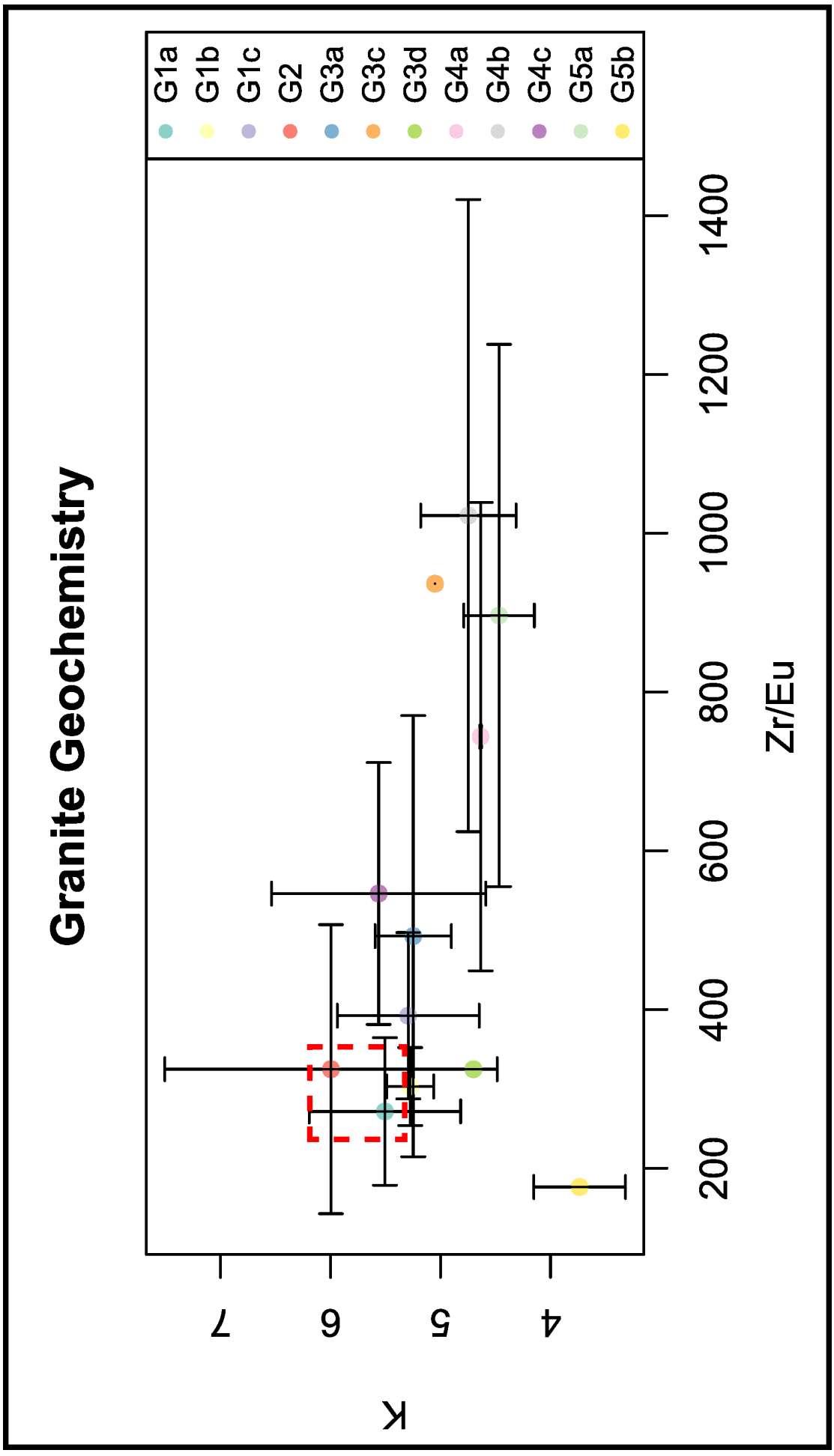
Granite Geochemistry
G1a
G1b
G1c
G2
G3a
G3c
G3d
G4a
G4b
G4c
G5a
G5b
K
4
5
6
7
Zr/Eu
200
400
600
800
1000
1200
1400

Figure 7

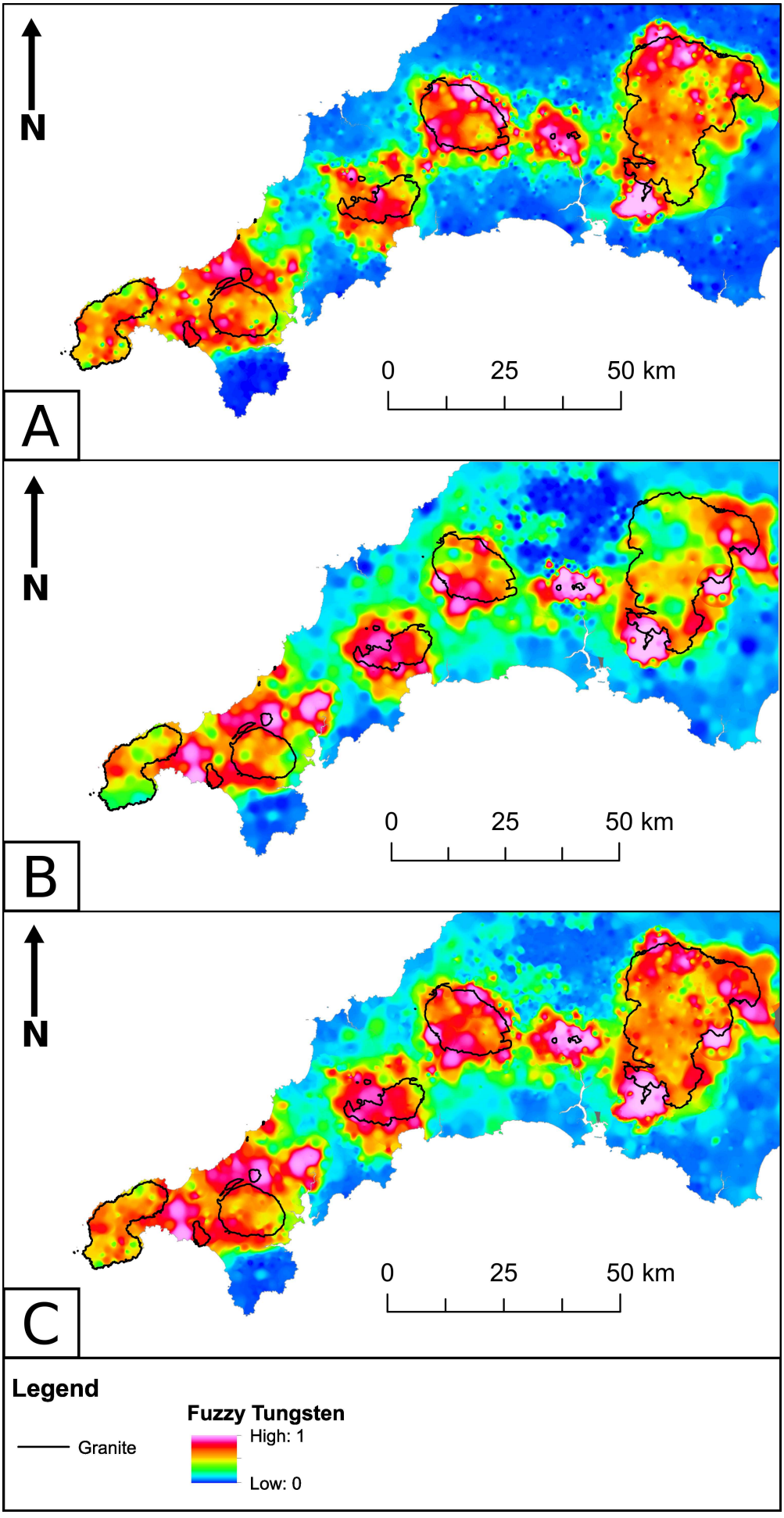
N
0
25
50 km
A
N
0
25
50 km
B
N
0
25
50 km
C
Legend
Granite
Fuzzy Tungsten
High: 1
Low: 0

Figure 8

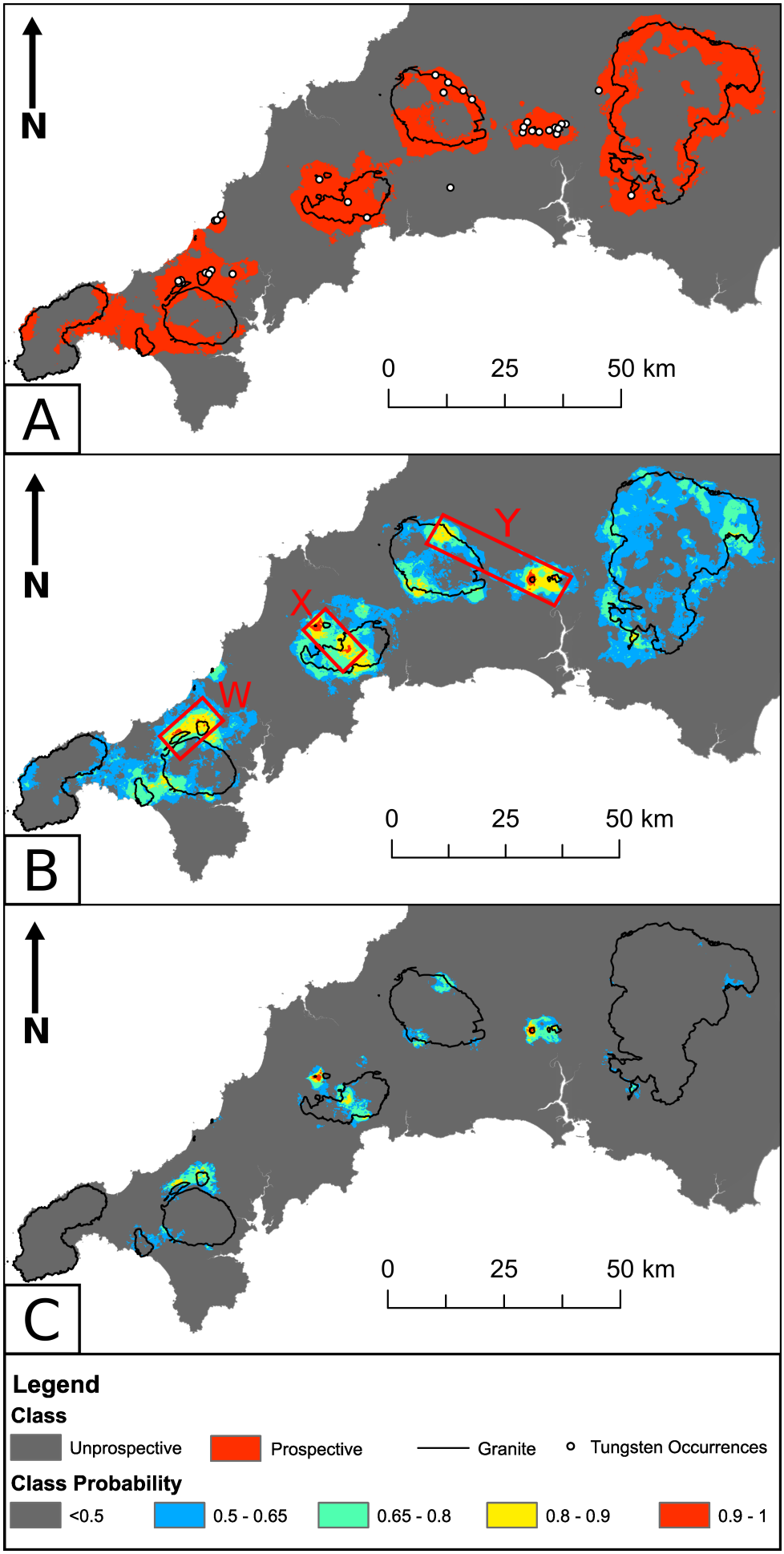
N
0
25
50 km
A
N
Y
X
W
0
25
50 km
B
N
0
25
50 km
C
Legend
Class
Unprospective
Prospective
Granite
Tungsten Occurrences
Class Probability
<0.5
0.5 - 0.65
0.65 - 0.8
0.8 - 0.9
0.9 - 1

Figure 9

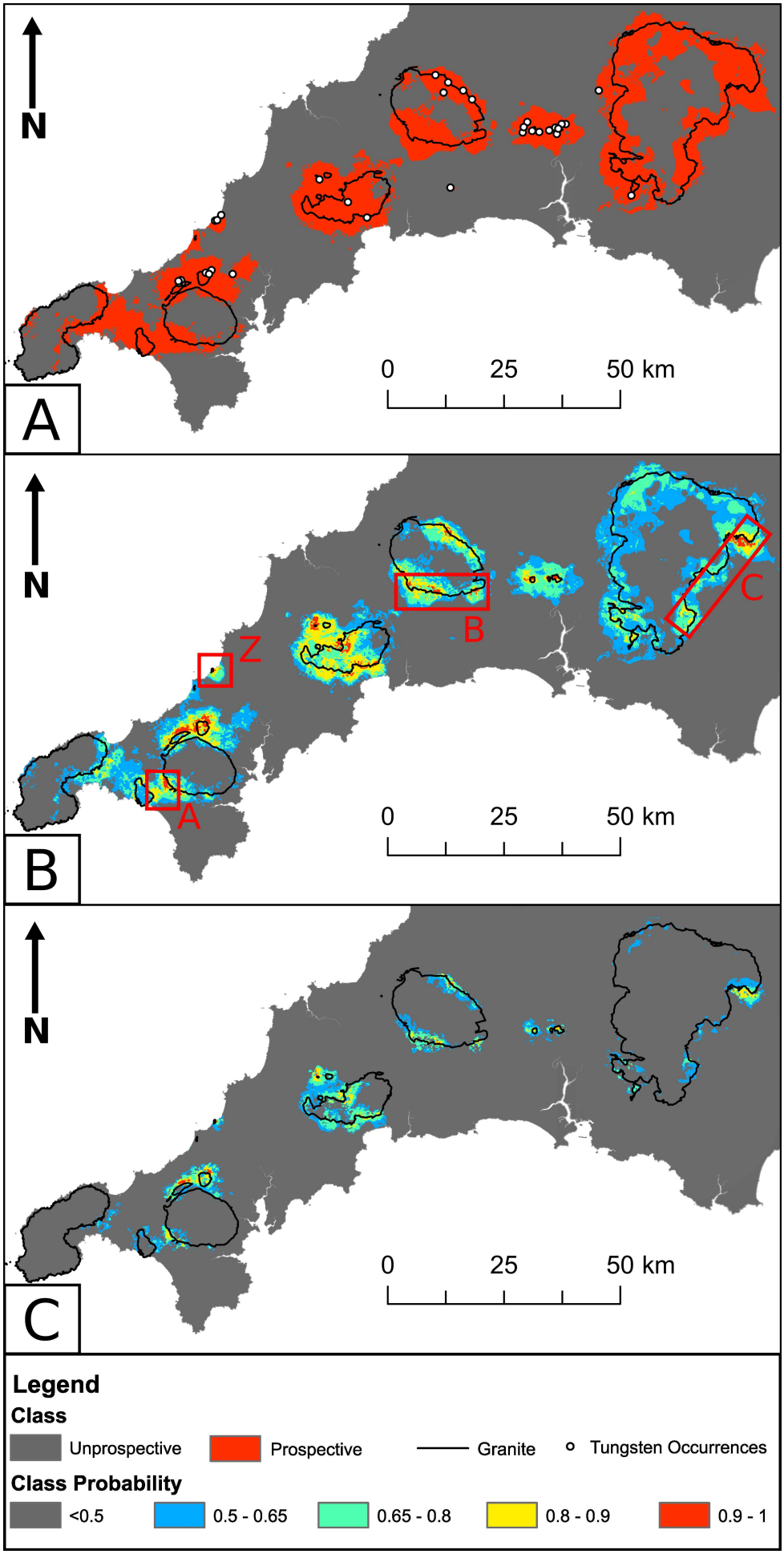
N
0
25
50 km
A
N
Z
B
C
A
0
25
50 km
B
N
0
25
50 km
C
Legend
Class
Unprospective
Prospective
Granite
Tungsten Occurrences
Class Probability
<0.5
0.5 - 0.65
0.65 - 0.8
0.8 - 0.9
0.9 - 1

Figure 10

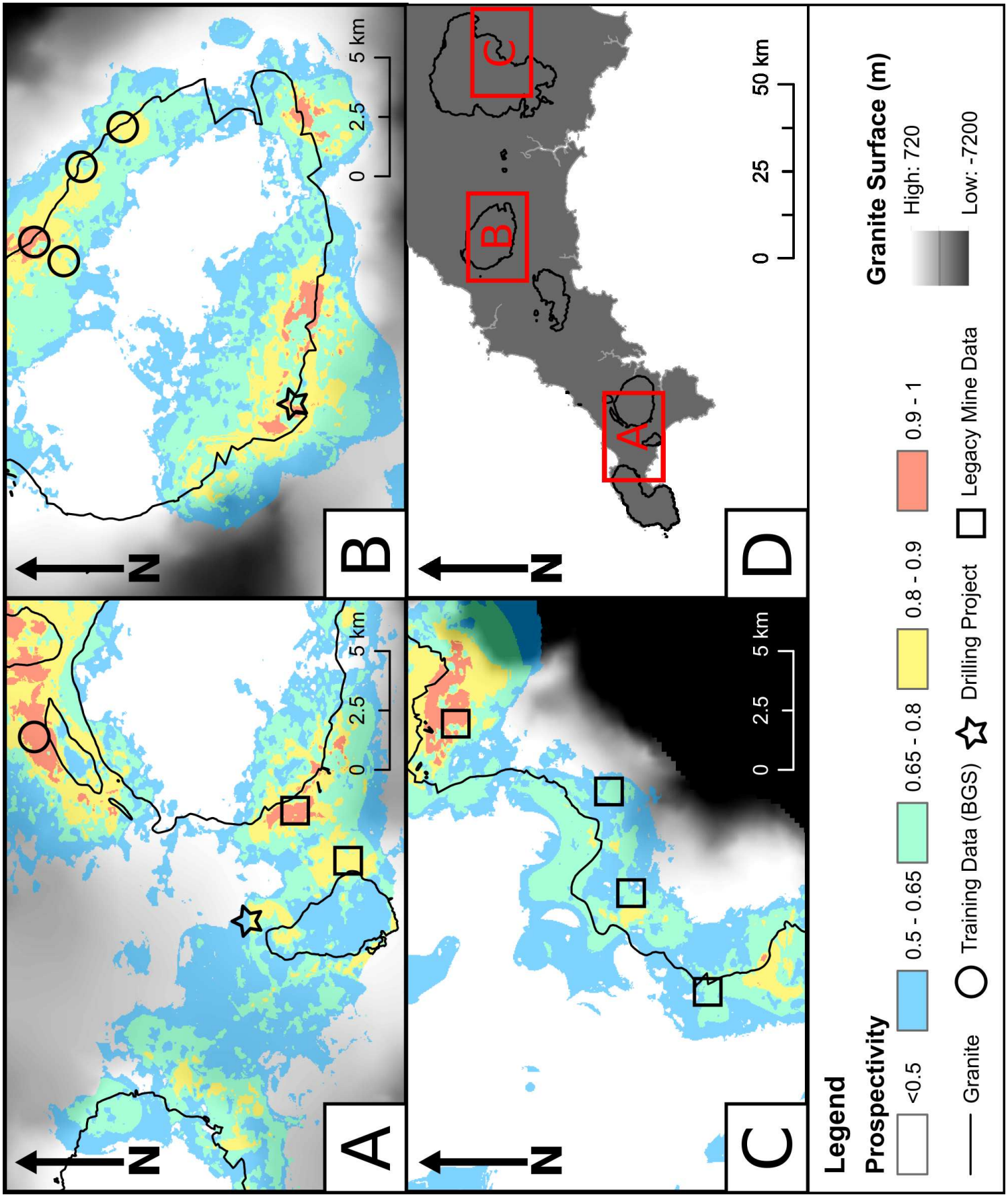
A
B
C
D
N
0 2.5 5 km
0 25 50 km
Legend
Prospectivity
<0.5
0.5 - 0.65
0.65 - 0.8
0.8 - 0.9
0.9 - 1
Granite
Training Data (BGS)
Drilling Project
Legacy Mine Data
Granite Surface (m)
High: 720
Low: -7200

table 1

Phenomenon	Elements	Sources
Mineralisation	W, Sn, As, Bi, Sb	(Andrews et al., 1987; Ball et al., 2002; Newall, 1994; Newall and Newall, 1989)
Aureole Alteration	Rb, Cs, Na*, K/Rb*, K/Cs*, K/eU*	(Ball et al., 1984, 1998; Newall, 1994; Newall and Newall, 1989)
Granite Composition	Ti/Sn*, K/(Zr/Eu)	(Ball et al., 1984, 1998; Simons et al., 2016)

table 2

Evidence Layer	Midpoint	Spread	Func.	Mean	SD
Proximity-to Granite in Z	N/A	N/A	TOC	0.814	0.039
Proximity-to Granite in XY	2750	2	Small	0.887	0.03
Density all lines	0.478	4	Large	0.638	0.062
Proximity-to lines	2713.41	2	Small	0.577	0.055
Airborne K/eU ratio	0.7	10	Small	0.666	0.055
Geochem Soil W	7.08	2	Large	0.887	0.032
Geochem Soil Sn	57.57	3	Large	0.829	0.034
Geochem Soil As	55.08	2	Large	0.819	0.038
Geochem Soil Bi	1.4	2	Large	0.819	0.032
Geochem Soil Sb	2.83	2	Large	0.49	0.052
Geochem Soil Rb	159.46	3	Large	0.708	0.051
Geochem Soil Cs	16.36	3	Large	0.749	0.035
Geochem Soil Na	0.83	6	Small	0.701	0.057
Geochem Soil K/Cs	0.22	3	Small	0.764	0.029
Geochem Soil K/Rb	0.02	5	Small	0.751	0.051
Geochem Soil Ti/Sn	0.08	2	Small	0.824	0.037
Geochem Stream-sediment W	27.47	1	Large	0.874	0.031
Geochem Stream-sediment Sn	636.63	1	Large	0.722	0.057
Geochem Stream-sediment As	117.68	1	Large	0.824	0.032
Geochem Stream-sediment Bi	2.86	2	Large	0.809	0.032
Geochem Stream-sediment Sb	2.69	1	Large	0.594	0.036
Geochem Stream-sediment Rb	176.41	4	Large	0.644	0.045
Geochem Stream-sediment Cs	20.35	3	Large	0.69	0.047
Geochem Stream-sediment Na	6359.1	5	Small	0.709	0.052
Geochem Stream-sediment K/Cs	1813	3	Small	0.533	0.042
Geochem Stream-sediment K/Rb	157.63	5	Small	0.668	0.058
Geochem Stream-sediment Ti/Sn	387.78	2	Small	0.706	0.064
Geochem Stream-sediment K/(Zr/Eu)	136.02	2	Small	0.739	0.044

table 3

Element or Ratio	Func.	Mean	SD	Soil	SS	Improvement in AUC
W	OR	0.901	0.026	0.887	0.874	INCREASE
Sn	OR	0.816	0.034	0.829	0.722	INCREASE
As	OR	0.851	0.033	0.819	0.824	INCREASE
Bi	OR	0.819	0.032	0.819	0.809	NO CHANGE
Sb	OR	0.537	0.085	0.49	0.594	DECREASE
Rb	OR	0.657	0.13	0.708	0.644	DECREASE
Cs	OR	0.71	0.037	0.749	0.69	DECREASE
Na	OR	0.758	0.048	0.701	0.709	INCREASE
K/Cs	OR	0.676	0.04	0.764	0.533	DECREASE
K/Rb	OR	0.713	0.055	0.751	0.668	DECREASE
Ti/Sn	OR	0.724	0.061	0.824	0.706	DECREASE

table 4

Model Type	Input Layers	Key Parameters	Mean	SD
Random Forest (standardised variables)	All evidence layers with zero mean and equal variance	mtry = 5; ntree = 20 000	0.959	0.03
Random Forest (fuzzy-transformed variables)	All fuzzy evidence layers, including geochemical data merged using the *fuzzy OR* operator	mtry = 4; ntree = 20 000	0.96	0.04

table 5

	Fuzzy-transformed model				Standardised model			
Class	**Σ Prob**	**Prob (%)**	**Σ Conf**	**Conf (%)**	**Σ Prob**	**Prob (%)**	**Σ Conf**	**Conf (%)**
<0.5	4597.3	76.58	5693.2	94.83	4526.6	75.4	5811.73	96.81
0.5-0.65	723.88	12.06	174.02	2.9	969.72	16.15	106.61	1.78
0.65-0.8	460.3	7.67	104.73	1.74	386.5	6.44	67.89	1.13
0.8-0.9	188.33	3.14	28.74	0.48	108.59	1.81	14.1	0.23
0.9-1.0	33.67	0.56	2.82	0.05	12.07	0.2	3.21	0.05
Total	6003.47	100	6003.52	100	6003.47	100	6003.54	100

e-component

Declaration of Interest Statement

Declaration of interests

☒ The authors declare that they have no known competing financial interests or personal relationships that could have appeared to influence the work reported in this paper.

☐The authors declare the following financial interests/personal relationships which may be considered as potential competing interests:

Nothing to declare